# New geological and geochronological constraints on the evolution of the Cotacachi - Cuicocha volcanic complex (Ecuador)

Marco Almeida Vaca, Mathilde Bablon, S. Daniel Andrade, Silvana Hidalgo, Xavier Quidelleur, Francisco Vasconez, Anais Vásconez Müller, Pierre Lahitte, Pablo Samaniego

# New geological and geochronological constraints on the evolution of the Cotacachi - Cuicocha Volcanic Complex (Ecuador)

*Marco Almeida Vaca[1], Mathilde Bablon[2,3], S. Daniel Andrade[1], Silvana Hidalgo[1], Xavier Quidelleur[2], Francisco J. Vasconez[1], Anais Vásconez Müller[1], Pierre Lahitte[2], Pablo Samaniego[4]*

[1] *Instituto Geofísico, Escuela Politécnica Nacional, Ap. 17-01-2759, Quito, Ecuador.*

[2] *Université Paris-Saclay, CNRS, GEOPS, Orsay, 91405, France.*

[3] *Université Côte d'Azur, CNRS, IRD, Observatoire de la Côte d'Azur, Géoazur, Valbonne, France*

[4] *Laboratoire Magmas et Volcans, Université Clermont Auvergne - CNRS - IRD, 6 Avenue Blaise Pascal, 63178 Aubière, France.*

## Abstract

Extensive fieldwork at the Cotacachi-Cuicocha Volcanic Complex (CCVC, North of Ecuador) resulted in a new collection of geological data including cartography, chronology, petrography, geochemistry, and morphology. This volcanic complex is formed by a central volcano (Cotacachi: 4939 m asl, current bulk volume of 56 ± 4 $km^3$), several peripheral domes, and a 3 km wide volcanic caldera (Cuicocha: 4.2 ± 0.1 $km^3$). CCVC comprises three stratigraphic members: The first, Cotacachi Basal, represents the initial phase of construction, which started at 173 ± 4 ka with a basal andesitic lava flow succession (~500 m-thick) including isolated basaltic-andesitic lavas (Verde Tola unit; NE: 113 ± 6 ka, SE: 133 ± 9 ka), the construction of some peripheral amphibole-bearing andesitic domes, such as Muyurcu and Loma Negra (138 ± 4 ka and <108 ka, respectively), and a debris-avalanche deposit to the north-west (0.5 - 1.8 $km^3$, older than 108 ka). The second member, Upper Cotacachi, consists of an andesitic lava flow succession (~300 m-thick), younger than 108 ± 6 ka. A gap of activity occurred afterwards from 100 to 70 ka, during which a second debris-avalanche (0.2 - 1.1 $km^3$, 108 to 65 ka) occurred to the NE, followed by the effusion of the dacitic Piribuela dome (65 ± 2 ka). Afterwards, several superimposed andesitic lava flows were emplaced at the summit, possibly around 15 - 10 ka since they lack glacial erosion. The third member includes the extrusion of the andesitic Cuicocha pre-caldera domes, which marks the beginning of a new eruptive stage of activity of CCVC during the Holocene, resulting in a violent eruption (3525 ± 35 to 2980 ± 30 a BP; VEI= 5) that partially destroyed the young dome and formed a funnel-shaped caldera (Cuicocha Caldera-Lake), ending with the emplacement of the Wolf and Yerovi post-caldera domes.

## 1. INTRODUCTION

The Cotacachi-Cuicocha Volcanic Complex (CCVC: 0.361°N, 78. 349°W), one of the largest volcanic centres in the northern part of the Ecuadorian Andes, is located ~50 km north of Quito. Its southern flanks are covered by pyroclastic deposits related to the Cuicocha caldera-forming eruption, which is one of the most explosive events to have occurred in the Ecuadorian volcanic arc during the Holocene (von Hillebrandt, 1989; Hall and Mothes, 1994; Pidgen, 2014). Highly populated (approx. thirteen thousand inhabitants - *https://www.ecuadorencifras.gob.ec/base-de-datos-censo-de-poblacion-y-vivienda/*) towns like Cotacachi, Quiroga, and Imantag have developed on top of these deposits without considering the hazards related to living close to a potentially active volcano.

Over the last decades, large explosive eruptions have occurred worldwide (e.g., Chaitén 2008, Lara et al., 2009; El Reventador 2002, Hall et al., 2004; Mt. Pinatubo 1991, Newhall and Punongbayan, 1996; among others) highlighting the importance of understanding the eruptive chronology of poorly known volcanic centres or complexes such as Cotacachi-Cuicocha; especially if they have displayed highly explosive activity in the past and are in close proximity to a large population.

During the past thirty years, the IG-EPN (Instituto Geofísico, Escuela Politécnica Nacional, Ecuador) and the IRD (Institut de Recherche pour le Développement, France) have conducted several studies intended to reconstruct the eruptive chronology of the main Ecuadorian volcanic centres, such as Chachimbiro (Bernard et al., 2014), Cayambe (Samaniego et al., 1998; Samaniego et al., 2005), Imbabura (Le Pennec et al., 2011; Andrade et al., 2019), Cotopaxi (Hall and Mothes, 2008), Antisana (Hall et al., 2017), Pichincha (Robin et al., 2010), Pululahua (Andrade et al., 2021; Vásconez Müller et al., 2022), Atacazo-Ninahuilca (Hidalgo et al., 2008), Tungurahua (Hall et al., 1999; Bablon et al., 2018), Chimborazo (Samaniego et al., 2012), Carihuairazo (Samaniego et al., 2022), Sangay (Monzier et al., 1999, Valverde et al., 2021), and others along the Ecuadorian Volcanic Arc (Bablon et al., 2020). These studies aim a better understanding of the development of the Ecuadorian arc volcanoes and strongly contribute to volcanic hazards assessment.

This work is part of this long-term program and aim to fill a gap concerning the Cotacachi-Cuicocha eruptive chronology.

Previous unpublished research has been mainly devoted to the Cuicocha caldera-forming eruption products (von Hillebrandt, 1989; Pidgen, 2014), and more recently to the current gas emissions observed in the caldera lake (Sierra et al., 2020; Melián et al., 2021). Indeed, Cuicocha volcano seismic and degassing activity is closely monitored by the Instituto Geofísico of the Escuela Politécnica Nacional University (IG-EPN) from Ecuador (Sierra et al., 2020). However, despite its proximity to densely populated areas, the eruptive history of the CCVC remains poorly documented. The purpose of this work is to provide a first geological map of the whole volcanic complex to address the lack of knowledge about the evolution of CCVC, based on new chronological, petrographic, and chemical data collection.

## 2. GEOLOGICAL CONTEXT

### 2.1. Geodynamical and geological context

The Ecuadorian volcanic arc results from the subduction of the oceanic Nazca plate beneath the South American continental plate (Hall and Wood, 1985; Barberi et al., 1988), with a convergence rate of 56 $mm.yr^{-1}$ (relative to the stable Brazilian shield; Trenkamp et al., 2002; Nocquet et al., 2014; Fig. 1). As a result, the Ecuadorian Arc is divided into four north-south volcanic alignments, which are located along the main morpho-structural domains (i.e., Western Cordillera, Inter-Andean Valley, Eastern Cordillera, and the sub-Andean zone; Hall et al., 2008). The CCVC is constructed on the Western Cordillera basement, a Late Cretaceous mafic volcanic complex (Pallatanga and Río Cala units; Fig. 2) and related sedimentary rocks (Natividad Unit; Fig. 2). These basement is interpreted as a part of the Caribbean-Colombian Oceanic Plateau with overlapping deposits of an intra-oceanic magmatic arc sequence, accreted to the continental margin during the Late Cretaceous (Goosens and Rose, 1973; Feininger and Bristow, 1980; Hughes and Pilatasig, 2002; Kerr et al., 2002; Jaillard et al., 2004; Pratt et al., 2005; Spikings et al., 2005; Luzieux et al., 2006, Vallejo et al., 2006, Vallejo et al., 2009, Vallejo et al., 2019). These mafic terrains also present quartz-diorite intrusions such as the Apuela batholith, dated at

16.5 ± 1.1 Ma (van Thournout, 1992; Boland et al., 2000. Fig. 2). Finally, the Late Oligocene – Early Miocene Silante formation (Vallejo et al., 2020) closes off the basement sequence bellow Cotacachi and consists of a succession of continental volcaniclastic sediments (Hughes and Bermudez, 1997; van Thournout, 1992; Boland et al., 2000).

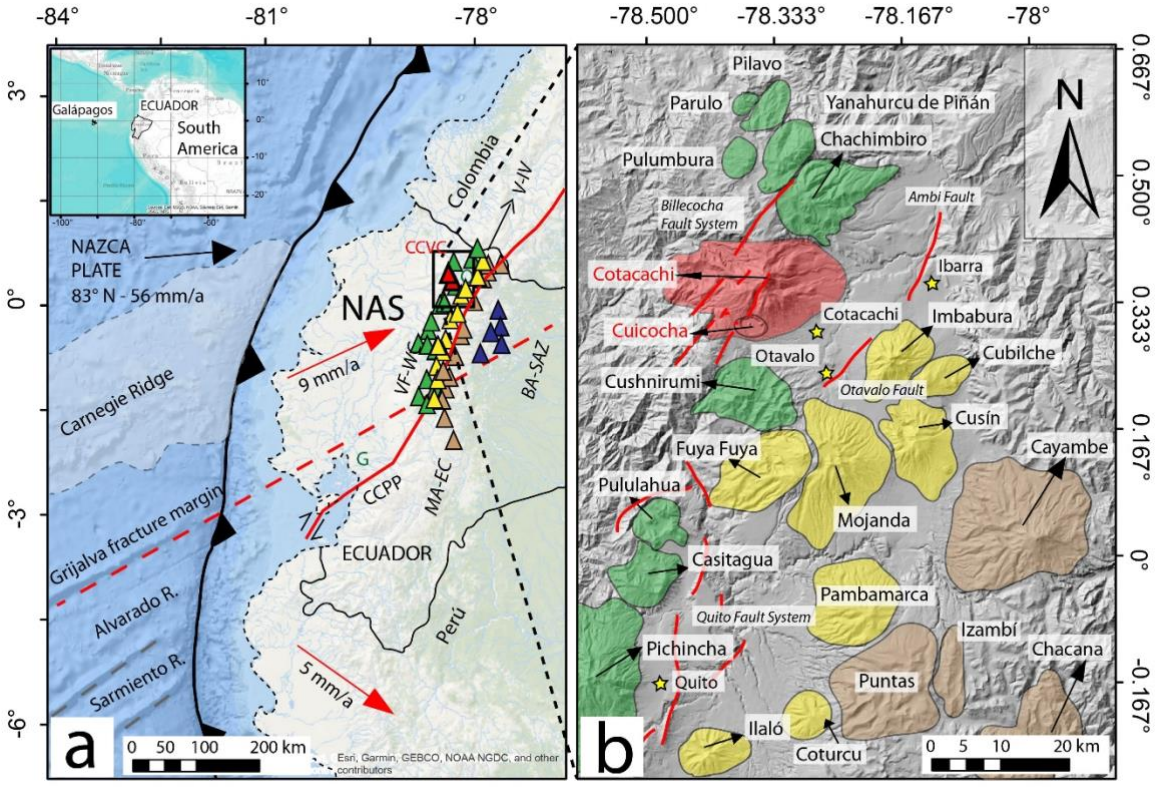


*Figure 1. a) Geodynamic context of the Ecuadorian volcanic arc (modified from Yepes et al., 2016) and the spatial location of the four volcanic alignments (Bernard and Andrade, 2011; Hall et al., 2008). VF-WC: volcanic front of the Western Cordillera (green, red triangles for Cotacachi and Cuicocha volcanoes), V-IV: volcanoes of the Inter-Andean Valley (yellow), MA-EC: the main arc of the Eastern Cordillera (brown), and BA-SAZ: the rear arc of the Sub-Andean zone (blue). The main morpho-tectonic structures are NAS (North Andean Sliver), CCPP (fault system of Chingual-Cosanga-Pallatanga-Puná), and the Billecocha, Huayrapungo and Quito fault systems (Ego et al., 1996; Eguez et al., 2003; Jomard et al., 2021), and Río Ambi and Otavalo faults (Alvarado et al., 2016; Andrade et al., 2019); G: City of Guayaquil. b) Close-up view of the CCVC area, with the different volcanic systems colored as in a). Active faults from the Billecocha Fault System are shown with red lines, and cities are located with a yellow star.*

## 2.2. Neotectonic context: the Billecocha Fault System (BFS)

The Billecocha Fault System (BFS. Ego et al., 1996; Eguez et al., 2003; Jomard et al., 2021; Figs. 1 and 2) appears as an eroded plateau-like morphology over the moorlands north of Cotacachi volcano (Fig. 3a), close to Cristococha Lake (Fig. 2 and 3b). The present morphology of the moorlands is related to the last glaciation (ca. 14 - 33 ka; Clapperton, 1990) and subsequent levelling out by the deposition of volcanic deposits during the Holocene (Ego, 1996). The Billecocha Plateau and its surrounding volcanoes are heavily affected by active faulting characterized by straight, sharp, and discontinuous scarps (Jomard et al., 2021). These structures possibly accommodate the convergence stresses of the Nazca plate subduction beneath South America through the suture planes of the Cretaceous-Eocene accretions (Boland et al., 2000; Hughes and Pilatasig, 2002). In this context, the BFS could correspond to a surface expression of a tectonic reactivation of the Pujilí Suture (Baize et al., 2020; Jomard et al., 2021). The slip rate of Billecocha was constrained at around 2 mm/yr (Ego et al., 1996; Eguez et al., 2003). Despite being located within the North Andean Sliver (NAS), the Billecocha Fault System has no direct relation to neither the NAS stress regime nor to the Chingual-Cosanga-Pallatanga-Puná (CCPP; Fig. 1) fault system (slip rate of 8-10 mm/yr; Nocquet et al., 2014; Alvarado et al., 2016). The approximate length of the Billecocha fault system is 6-7 km, striking approximately north 25° and dipping to the south-east (Eguez et al., 2003). This structure has also been considered as a normal fault due to the presence of scarps, sag-ponds, and drainage cuts (Ego et al., 1996; Eguez et al., 2003). The morphology of the fault scarp and some detailed studies of kinematics and chronology in the associated stratigraphy suggest that its last movement occurred between 5.7 and 10 ka (Ego et al., 1996, Eguez et al., 2003). This assumption was corroborated by Jomard et al. (2021), who mention that the current activity of this fault system is low.

## 3. ANALYTICAL METHODS

Several field campaigns resulted in the detailed study of 79 outcrops (Appendix table A and appendix figure A.1) related to the Cotacachi-Cuicocha Volcanic Complex. Fieldwork included geological mapping (1:25.000 scale) and sampling of the

principal stratigraphic units, resulting in a collection of 52 unaltered samples for geochronological, petrographic, and geochemical analyses.

### 3.1. Geochronology

Considering the volcano stratigraphy, as well as the sample freshness and their low vesicularity, we selected 9 lava samples and one juvenile block from a block-and-ash-flow deposit. These samples were dated using the potassium-argon (K-Ar) method (Table. 1a) with the unspiked Cassignol-Gillot technique (Cassignol and Gillot, 1982; Gillot et al., 2006), which was shown to be suitable for calc-alkaline samples from Quaternary arc volcanoes (e.g., Germa et al., 2011; Ricci et al., 2015; Bablon et al., 2018). This technique determines the radiogenic argon ($^{40}Ar^{*}$) content of the sample and compares the $^{40}Ar/^{36}Ar$ ratios of both the sample and the atmosphere measured in the same condition. Since the groundmass of a lava flow is the last phase to crystallize when it cools after being erupted, its initial $^{40}Ar/^{36}Ar$ ratio corresponds to that of the atmosphere (*i.e.,* it does not contain any excess $^{40}Ar^{*}$). On the contrary, phenocrysts such as plagioclase or biotite can carry inherited $^{40}Ar$ that could significantly bias ages towards older values (e.g., Harford et al., 2002; Samper et al., 2008). Therefore, we carried out our measurements on groundmass, after removing phenocrysts using heavy liquids and magnetic separations. One measurement was carried out on separated plagioclase crystals to compare the result with the age obtained on groundmass. Details of analytical procedures, decay constants, standards used, and uncertainty calculations are given in Bablon et al. (2018). Both potassium and argon measurements were carried out at the GEOPS laboratory at Orsay (Paris-Saclay University, France) using an Agilent 240 Series AA flame absorption spectrometer and a multi-collector 180° sector mass spectrometer, respectively. Measurements were performed at least twice to check their reproducibility within their uncertainty range, at the 1σ level. Final ages and uncertainties were calculated by averaging each analysis, weighted by their $^{40}Ar^{*}$ content.

The age of Cuicocha caldera explosive sequence was constrained by five new radiocarbon ages obtained from charcoal and soil samples collected from pyroclastic

deposits. These samples were analysed at the Center for Isotope Research (CIO), Groningen University (The Netherlands). Table 1b compiles the sample chronology with conventional $^{14}C$ ages (±1σ) as well as calibrated ages (± 1σ and 2σ). Conversion from conventional $^{14}C$ ages to standard and calendar ages was carried out using the Calib 7.1 code (Stuiver and Reimer, 1993; Stuiver et al., 2005) and the Northern Hemisphere calibration curve (IntCal20, Reimer et al., 2020).

### 3.2. Petrography and geochemistry

Thin sections of 52 samples were used to establish the samples petrography (modal counting, texture, and structures) using a petrographic microscope (ZEISS AXIO Scope A1; Appendix table B.1). Whole-rock chemical analyses of major and trace elements for 61 samples spanning the entire volcanic history were carried out at the Laboratoire Geo-Ocean (IUEM-UBO, Brest, France; Appendix table B.2). Measurements were performed on agate-crushed powders by ICP-AES (Inductively Coupled Plasma – Atomic Emission Spectroscopy). The relative standard deviation is 1% for $SiO_2$ and 2% for the other major elements, except for low concentrations (<0.50%) for which the absolute standard deviation is 0.01%. The analytical procedure is described in Cotten et al. (1995).

### 3.3. Edifice volume, construction and erosion rates estimates.

To quantify the morphological characteristics of this volcanic complex, we used two digital elevation models (DEM), one developed by the Instituto Geográfico Militar (IGM) of 30-m resolution, and a second model of 4-m resolution from SIGTIERRAS project, by the Ministry of Agriculture and Livestock (https://www.agricultura.gob.ec/sigtierras/). In this study, we used the 30-m for regional (e.g., for traces of regional fault systems and description of the morphology of stratigraphic units) and the 4-m one for local analyses (e.g., identification of small volcanic structures as land-scarps, estimation of slopes and volume calculations).
Quantification of the minimum edifice volume, reconstruction, and erosion rate estimates were performed in two different ways: The first method for volume

estimation considers linear interpolation using a MATLAB ® script, which applies the volcano's baseline to create an interpolated grid that depicts the underlying basement (Table 2a). This method does neither consider those parts underneath the observed base nor those that were already eroded (see Andrade et al., 2021). In contrast, the second method, developed by Lahitte et al. (2012), and further improved by Germa et al. (2015), uses the ShapeVolc algorithm and ArcGis software to make numerical surface interpolations based on the present-day topography of the basement and the CCVC's crest elevations (Table 2b). It consists of numerical modelling of the pre-erosional shape of the volcano, based on the extrapolation of the uneroded surfaces such as crests (Dibacto et al., 2020).

## 4. RESULTS

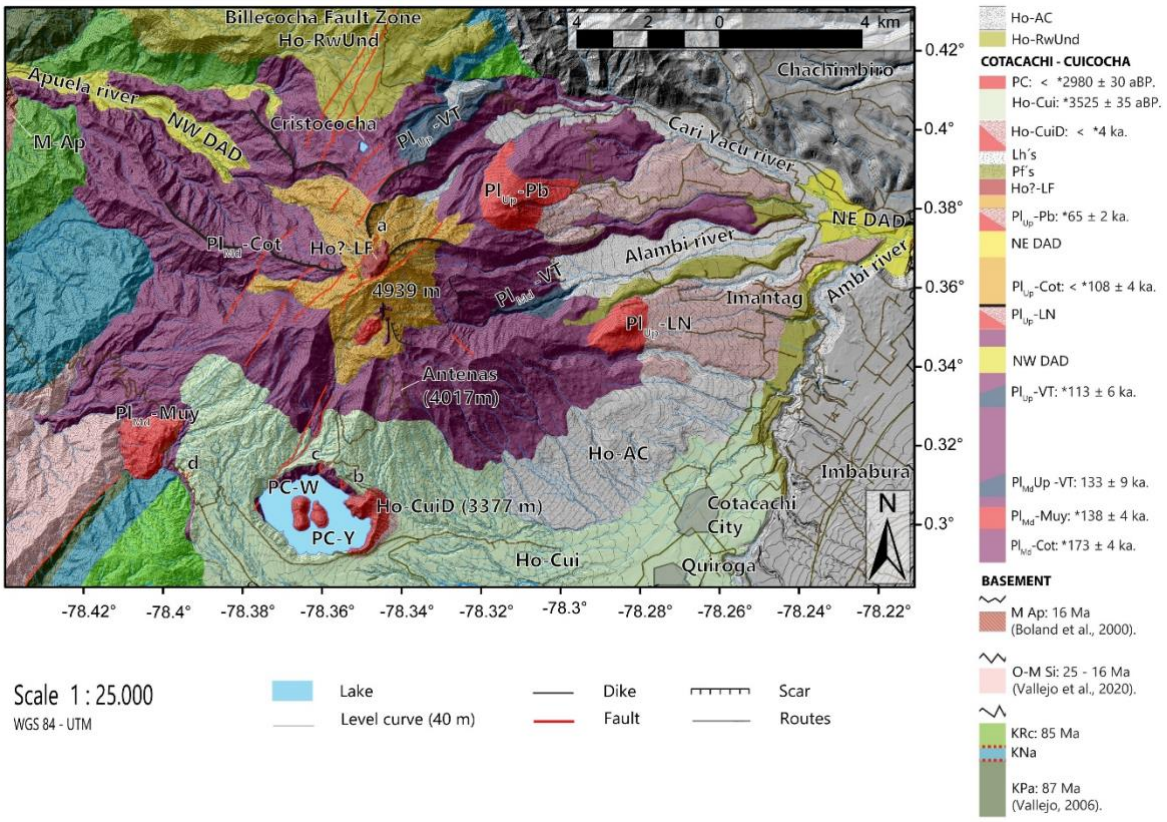


*Figure 2. Geological map of the Cotacachi-Cuicocha volcanic complex. Ho-AC: Alluvial and colluvial deposits. Ho-RwUnd: Undifferentiated, reworked volcaniclastic deposits. PC: Post-caldera Domes (W: Wolf, Y: Yerovi). Ho-Cui: Cuicocha pyroclastic density currents. Ho-CuiD: Cuicocha pre-caldera / block and ash deposits. HO? -LF: Lava flows of the summit. Lh´s: Lahar deposits of Cotacachi. Pf´s: Pyroclastic deposits of Cotacachi. Summit lava flows. PlUp-Pb: Piribuela dome / block and ash*

*deposits. NE DAD: Northeastern debris avalanche deposit. PlUp-LN: Loma Negra dome / block and ash deposits. PlUp-Cot: Upper Cotacachi Member. NW DAD: Northwestern debris avalanche deposit. PlMd-Up-VT: Verde Tola Unit. PlMd-Muy: Muyurcu dome. PlMd-Cot: Basal Cotacachi Member. MioAp: Apuela batholith. EOSi: Silante Unit. KRc: Río Cala Unit. KNa: Natividad Unit. KPa: Pallatanga Unit. Letters: a, b, c and d are related to the locations of figure 5 outcrops of neotectonics.* ***** *For the new ages obtained during this study.*

### 4.1. Morphology and structure of CCVC

The Cotacachi composite stratovolcano is the main edifice of the Cotacachi-Cuicocha volcanic complex. Its basal surface covers an area of ~268 km$^2$, with a north-south axis of 14-15 km and an east-west axis of 20-21 km (Figs. 2, 3). Cotacachi volcano lower flanks are characterized by smooth slopes (6° - 25°; Appendix figure A.2) and radial U-shaped glacial valleys, especially at the southern and eastern flanks, which are partially filled with moraine deposits as well as local and regional pyroclastic deposits. The moraines are in the high moorlands (between 3700 to 3800 m above sea level - asl) north of the edifice and are mostly visible around a small glacial lake called Cristococha (3777 m asl; Fig. 3b). The presence of radially oriented, deep glacial valleys, the frequent glacial striations displayed by basal lavas (Fig. 3c), and the associated moraines, have been attributed to the Late Pleistocene glaciations (Last Glacial Maximum - LGM), dated in the range of *ca.* 33 to 14 ka (Clapperton, 1990; Samaniego et al., 2012; Bablon et al., 2019) in this part of the Andes. Towards the top of the edifice, the upper Cotacachi flanks (Fig. 3a) are characterized by an abrupt change of slope (17° – 35°, Appendix figure A.2), sculpting a pyramidal structure strongly affected by glacial erosion processes. Indeed, the presence of smaller, young-looking moraines, reaching down to 3700 m asl suggests that the terminal Cotacachi edifice was also affected by the glacial advances younger than the LGM (i.e., the Younger Dryas and/or the Neoglacial event, roughly dated at 10-12 ka and ~5 ka respectively; Clapperton, 1990). The remnants of the last glaciers on the northern and eastern flanks of the volcano were reported by Whymper (1892), Wolf (1892), and Troya (1913). Towards Cotacachi volcano summit, on its southern flank, behind some relatively small hillside domes (Fig. 3d), two major peaks (4939 m asl and 4756 m asl, respectively) aligned north-

south stand out. These peaks delimit a crater, inside which a dome-like structure characterized by the absence of glacial erosion is observed (Fig. 3e).

Two groups of medium- to large-size scars of deep horse-shoe shaped depressions are present on the north-western and north-eastern flanks of Cotacachi (3 to 10 km wide; Appendix figure B). One is open towards the NW with a maximum width of 5-6 km, while the second open towards the NE with an opening of 6-7 km. The lava flows that constitute the main cone-building stage crop out at the inner walls of escarpments. Additionally, younger, and smaller (2-3 km, Appendix figure B, black coloured scars) scars were observed inside the largest one (Appendix figure B, blue coloured scars) and may correspond to landslides produced by gravitational processes or perhaps recent seismic activity (e.g., 7.0 – 7.3 M August 16$^{th}$, 1868 - Ibarra earthquake, Beauval et al., 2010; Madera,1918).

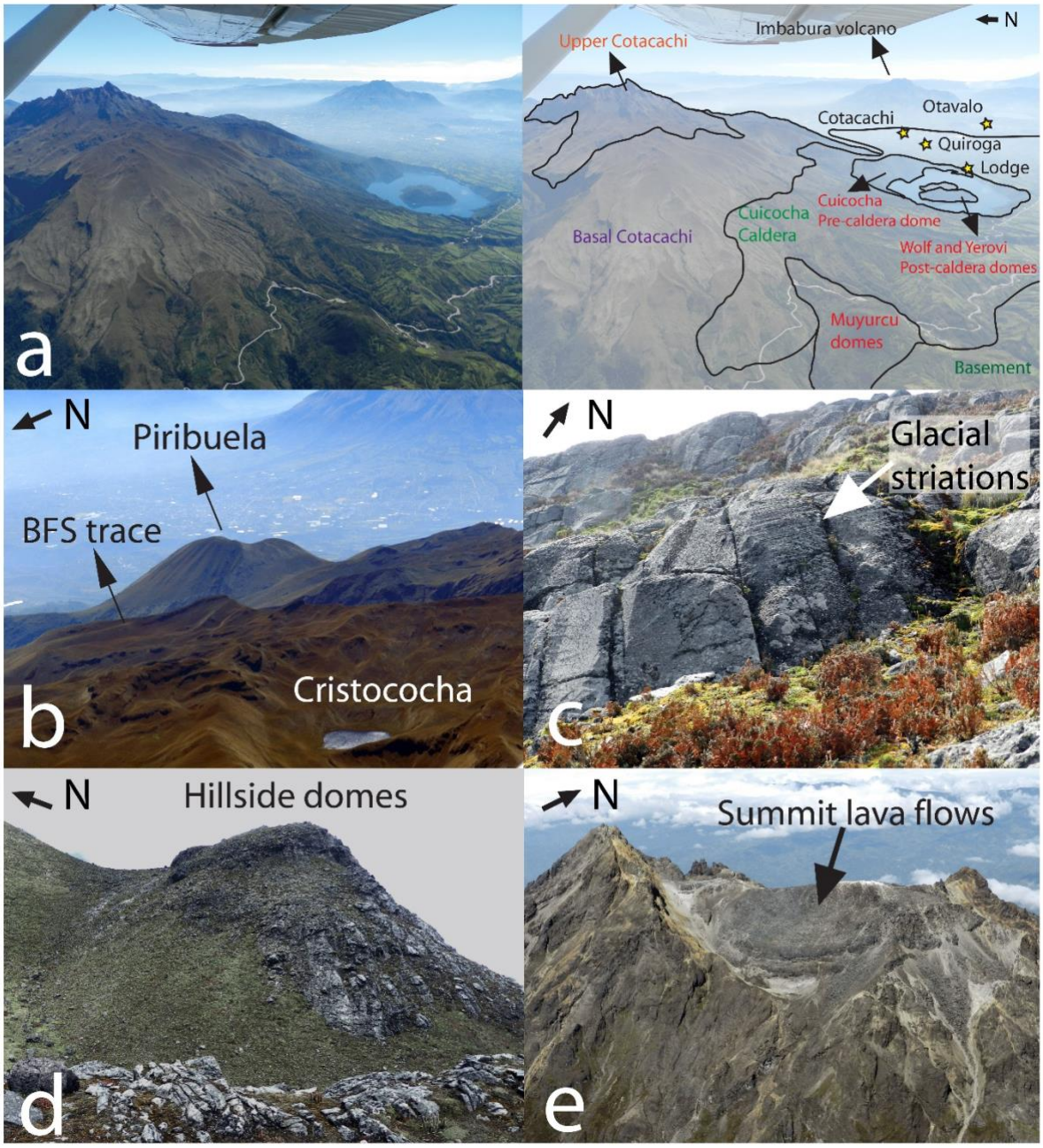


*Figure 3. a) Aerial photograph and illustration of the different stratigraphic members of the Cotacachi-Cuicocha volcanic complex. The yellow stars represent the populations closest to the volcanoes. b) Cristococha (0.396° N; 78.349° W) post-glacial lake and the different associated moraine deposits (between 3600 to 3900 m asl, on the north-western flanks of Cotacachi). c) Sub-horizontal glacial striated lava flows (0.350° N; 78.345 W) corresponding to basal Cotacachi (between 3450 to 4000 m asl, on the southern flank). d) Viscous lava flows (0.352° N; 78.346° W) forming a lava dome on the hillside southern flank of the volcano. e) Aerial photograph of the amphitheater of the Cotacachi volcano crater. Note the unglaciated summit lava flows (0.367° N; 78.346° W) or domes superimposed horizontally inside the crater.*

Moreover, several volcanic domes are distributed around the Basal Cotacachi edifice (Figs. 2, 4). Some of them are observed as compound domes (Muyurcu: 3502 m asl; Fig. 4a), and others as dome clusters (Loma Negra: 3066 m, Fig. 4b; Piribuela: 3871 m asl, Fig. 4c). In addition, the remnants of the Cuicocha pre-caldera dome (3377 m asl; Fig. 4d) are observed west of Cuicocha caldera (Fig. 2), which has an elliptical shape and reaches 3.2 km from east to west and 2.3 km from north to south. The caldera rim is limited by steep walls (55 to 90°, 5.1 $km^2$; Appendix figure A.2) which have been filled by almost 0.3 $km^3$ of a meteoric water lake, occupying a minimum area of 3-4 $km^2$ (Gunkel and Beulker, 2009). The maximum water depth is 148 m, with a mean depth of 72 m (Gunkel and Beulker, 2009). Two east-west aligned islets located in the centre of the caldera lake correspond to post-caldera domes (Fig. 2). These islets are named Wolf (3247 m asl) and Yerovi (3142 m asl) and cover 0.5 and 0.3 $km^2$ of the lake surface, respectively.

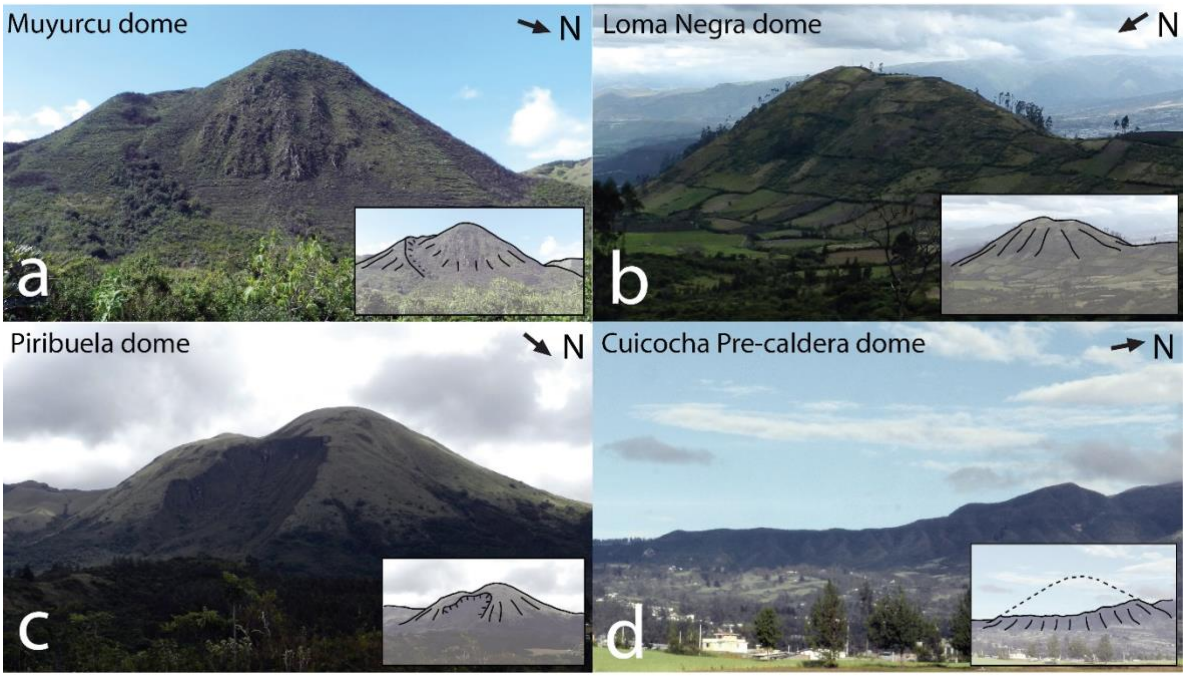


*Figure 4. Photographs of the peripheral domes of Cotacachi volcano (see Fig. 2 for geographic location). In chronological order: a) Muyurcu dome (0.323° N; 78.398° W), b) Loma Negra dome (0.351°N; 78.284° W), c) Piribuela dome (0.383° N; 78.314° W), and d) Cuicocha dome amphitheater (0.307° N; 78.348° W), observed from the east at the Selva Alegre – Quiroga road. Morphological features, as well as possible reconstruction of the Cuicocha dome and the scarp over the south-eastern flank of the Piribuela dome are shown as inserts at the bottom right.*

## 4.2. Main neo-tectonic structures of CCVC

Regional neo-tectonic structures of the Northern Andes cut across Cotacachi composite volcano (Fig. 5a). Lineaments along with rupture zones crop out at the western and northern walls of the Cuicocha caldera (Fig. 5b, 5c), extending across Cotacachi from the southwest to the northeast (N22°E, N45°E - dipping 30 to 35° N-NE). Displacements show apparent gravitational/extensional movements of the basal Cotacachi lavas. The lineaments and their associated fault kinematics were observed as trans-tensional/negative flower structure, and strike-slip faults with secondary normal components (Ego, 1996, Eguez et al., 2003, this study). Finally, the trace of the surface morphology looks like a horsetail structure (Fig. 2, Appendix figure B).

Outcrops along the Cuicocha – Apuela road, exhibit small faults with positive flower structures (Fig. 5d) with mostly compressive kinematics accompanied by some secondary gravitational structures, whose azimuth strikes similar to the NE – SW main Andean trend (Trenkamp et al., 2002; Eguez et al., 2003; Bourgois, 2013; Alvarado et al., 2016; Yepes et al., 2016). At this locality the faults propagate through the surge succession of Cuicocha caldera, a basal hydrothermally altered rock sequence, and the older Cotacachi lava flows.

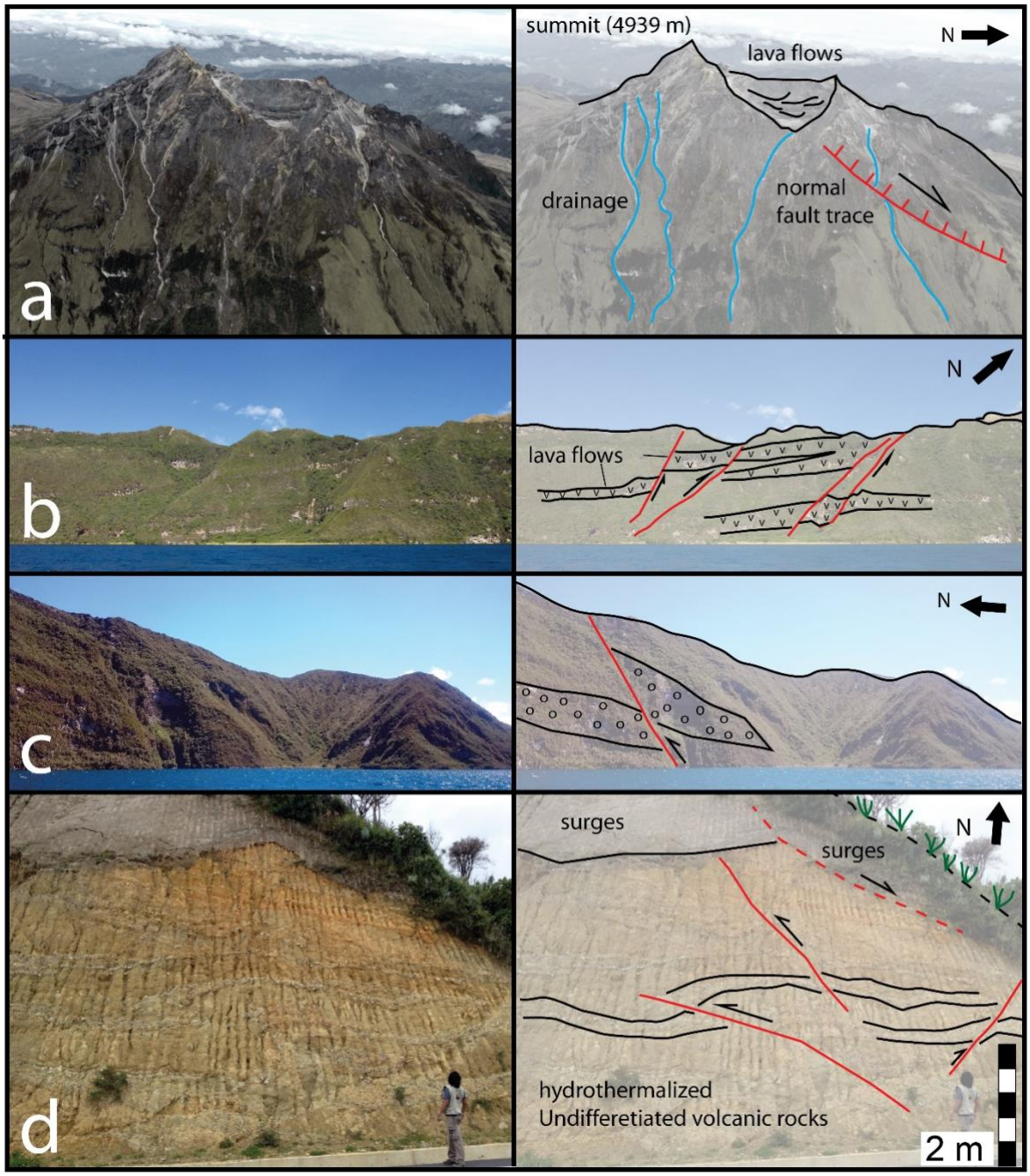


*Figure 5. Photographs of the different fault outcrops in the CCVC. The photographs and diagrams in two dimensions are shown according to the potential size of the structure: a) prolongation of the Billecocha fault system over the eastern flank (0.365° N; 78.339° W) of Cotacachi volcano edifice. The structure is observed as a normal type of fault with western vergence. The lava flows of the summit are not affected. b) northwestern wall (0.311° N; 78.373° W) of Cuicocha caldera lake, different structures of negative flower type are observed. c) northern wall (0.311° N; 78.354° W) of Cuicocha caldera lake, a potentially inverse structure is observed. d) structures of positive flower type (0.311° N; 78.394° W) in the Holocene deposits of Cuicocha, at the base of the surges some hydro-thermally altered and undifferentiated volcaniclastic deposits are observed.*

## 4.3. Chronology of the CCVC

***Cotacachi Basal member***

*Main basal lava flows ($Pl_{Md}$-Cot)*

Basal Cotacachi lava flows (purple unit in Fig. 2) are a monotonous, ~500 m-thick succession of sub-horizontal lava flows (Appendices figures C.1 and C.2), that reach up to 5-7 km from the summit. The most representative outcrops are located at the north-eastern and the south-western flanks of the volcano, between 2700 and 3900 m asl, as well as at the inner northern walls of the Cuicocha caldera. This succession rests discordantly on the Cretaceous-Paleogene volcanic basement, covering a surface of 107 $km^2$. Well-compacted matrix-supported breccias (30 vol.% of andesitic lithics) are interlayered between the lava flows. The lavas are porphyritic basaltic andesites and andesites (54.7 – 61.8 wt.% $SiO_2$), with a mineral assemblage comprising plagioclase (11 vol. %), clinopyroxene (5 vol. %), orthopyroxene (3 vol. %), and olivine (2 vol. %) (e.g., COTA-08). K-Ar ages obtained from two samples taken near the base of the Cotacachi basal lava flows yielded ages of 173 ± 4 and 163 ± 4 ka, respectively (COTA 54 and COTA-01, Table 1a and Appendix figure C.1). Three additional lava samples corresponding to the top of the basal lava flows yielded ages of 110 ± 6, 108 ± 6 and 108 ± 4 ka, respectively (COTA-05, CUI-28, and CUI-30A samples, Table 1a, Appendix figure C.1).

a

| Sample | Lab Code | Location | Longitude (m) | Latitude (m) | Member, Unit | Phase | K (%) | $^{40}Ar^{*}$ (%) | $^{40}Ar^{*}$ x $10^{11}$ (at/g) | Age ± 1σ (ka) | Mean age (ka) |
|---|---|---|---|---|---|---|---|---|---|---|---|
| COTA 54 | 17EQ86 | Distal lava flow, SW flank | 787198 | 10037876 | Basal Cotacachi | Groundmass | 1.510 | 4.72 | 2.6912 | 171 ± 4 | 173 ± 4 |
| | | | | | | | | 6.07 | 2.7518 | 174 ± 4 | |
| COTA 01 | | Lava flow, E valley | 798773 | 9838736 | Basal Cotacachi | Groundmass | 1.075 | 4.32 | 1.7989 | 160 ± 4 | 163 ± 4 |
| | | | | | | | | 4.38 | 1.8683 | 166 ± 4 | |
| COTA 56 | 17EQ88 | Muyurcu dome, SW flank | 789687 | 10035549 | Muyurcu dome | Groundmass | 1.378 | 3.60 | 2.0004 | 139 ± 4 | 138 ± 4 |
| | | | | | | | | 4.53 | 1.9669 | 137 ± 4 | |
| COTA 02 | | Lava flow, SE flank | 800141 | 9839050 | Verde Tola Unit | Groundmass | 0.952 | 1.53 | 1.3566 | 136 ± 9 | 133 ± 9 |
| | | | | | | | | 1.56 | 1.2926 | 130 ± 9 | |
| COTA 012 | | Proximal lava flow, S flank | 795416 | 10038627 | Upper Cotacachi | Groundmass | 2.001 | 5.33 | 2.5751 | 123 ± 3 | 122 ± 8 |
| | | | | | | | | 6.41 | 2.3856 | 114 ± 2 | |
| | | | | | | | | 5.68 | 2.7248 | 130 ± 3 | |
| COTA 60 | 17EQ93 | Distal lava flow, NE flank | 797793 | 10045132 | Verde Tola Unit | Groundmass | 1.133 | 1.77 | 1.4370 | 121 ± 7 | 113 ± 6 |
| | | | | | | | | 2.23 | 1.2733 | 108 ± 5 | |
| | | | | | | | | 2.12 | 1.3089 | 111 ± 5 | |
| COTA 05 | | Lava flow, E flank | 798715 | 9838058 | Basal Cotacachi | Groundmass | 1.175 | 2.13 | 1.3826 | 113 ± 6 | 110 ± 6 |
| | | | | | | | | 1.85 | 1.3150 | 107 ± 6 | |
| CUI 28 | | Lava flow, S flank | 796267 | 9836562 | Basal Cotacachi | Groundmass | 1.156 | 1.66 | 1.2859 | 107 ± 7 | 108 ± 6 |
| | | | | | | | | 2.40 | 1.3150 | 109 ± 5 | |
| CUI 30A | | Lava flow, S flank | 795354 | 9836039 | Basal Cotacachi | Groundmass | 1.522 | 2.68 | 1.7491 | 110 ± 4 | 108 ± 4 |
| | | | | | | | | 3.28 | 1.6799 | 106 ± 4 | |
| | | | | | | Plagioclase | 0.186 | 0.66 | 0.3353 | 173 ± 26 | 207 ± 25 |
| | | | | | | | | 0.97 | 0.4492 | 231 ± 24 | |
| COTA 26 | | Block from a PF deposit, NE flank | 801184 | 10041881 | Piribuela Dome | Groundmass | 2.529 | 3.88 | 1.7183 | 65 ± 2 | 65 ± 2 |
| | | | | | | | | 6.08 | 1.6972 | 64 ± 1 | |
| COTA 57 | 17EQ89 | Lava flow, Cuicocha dome | 795129 | 10032404 | Cuicocha | Groundmass | 1.302 | < 0.1 | -0.0092 | < 4 | < 4 |

b

| Sample | Lab code | Locality | Longitude (m) | Latitude (m) | Unit | Type of sample | 14C age (years BP) | d13C (o/oo) | Calendar age range (2 sigma) - InCAL20 (cal BP) | Relative area (%) | Calendar age range (1 sigma) - InCAL20 (cal BP) | Relative area (%) |
|---|---|---|---|---|---|---|---|---|---|---|---|---|
| **CUI-27C** | GrA 54410 | Organic soil under ash before surges | 796378 | 10037549 | Cuicocha | soil | 5750 ± 35 | -24.77 | 6449 - 6647 | 95 | 6584 - 6621 | 19 |
| | | | | | | | | | | | 6493 - 6565 | 50 |
| **CUI-22A** | GrA 54412 | Soil under pyroclastic flow | 790562 | 10034145 | Cuicocha | soil | 4470 ± 35 | -23.01 | 4973 - 5290 | 95 | 4986 - 5001 | 4 |
| | | | | | | | | | | | 5041 - 5070 | 10 |
| | | | | | | | | | | | 5102 - 5135 | 12 |
| | | | | | | | | | | | 5167 - 5279 | 43 |
| **CUI-27B** | GrA 54408 | Organic soil under surges | 796378 | 10037549 | Cuicocha | soil | 3525 ± 35 | -25.24 | 3895 - 3695 | 95 | 3863 - 3867 | 2 |
| | | | | | | | | | | | 3819 - 3849 | 19 |
| | | | | | | | | | | | 3722 - 3797 | 48 |
| **CUI-22B** | GrA 54411 | Pyroclastic flow and surges | 790562 | 10034145 | Cuicocha | charcoal | 2980 ± 30 | -26.00 | 3060 - 3249 | 92 | 3141 - 3210 | 46 |
| | | | | | | | | | 3301 - 3324 | 3 | 3107 - 3126 | 11 |
| | | | | | | | | | 3033 - 3040 | 1 | 3077 - 3094 | 11 |
| | | | | | | | | | 3008 - 3013 | 0 | | |
| **CUI-27A** | GrA 54406 | Soil under ash fall afther Cuicocha | 796378 | 10037549 | Cuicocha | soil | 2245 ± 30 | -25.71 | 2295 - 2339 | 28 | 2160 - 2166 | 3 |
| | | | | | | | | | 2152 - 2265 | 68 | 2177 - 2235 | 42 |
| | | | | | | | | | | | 2232 - 2301 | 23 |

Table 1. a) Potassium-argon (K-Ar) ages obtained in this study (see text for details). Column headings indicate sample name, lab code, outcrop location, member/unit, dated phase of the sample, potassium content in percent, radiogenic argon content in percent and in atoms per gram, age obtained for each measurement, weighted mean age in ka, given with 1-σ

368 uncertainty. Measurements were carried out on groundmass for all samples, and on plagioclase crystals for CUI 30A sample.
369 b) Radiocarbon ages obtained from charcoal and soil samples collected in pyroclastic deposits. 14C chronology table gives
370 the conventional ages (±1σ), and the calibrated ages (± 1σ and 2σ) to standard and calendar ages, using the Calib 7.1 code
371 (Stuiver and Reimer, 1993; Stuiver et al., 2005) and the Northern Hemisphere calibration curve (IntCal13, Reimer et al.,
372 2013; IntCal20, Reimer, 2020).

373 *Muyurcu domes unit ($Pl_{Md}$-Muy)*

374 Muyurcu (3502 m asl) (Fig. 4a) is a small (1.5 - 2 km in diameter, with a surface of
375 2.4 $km^2$) compound dome, which is located at the lower south-western flank of
376 Cotacachi (red unit in Fig. 2). Muyurcu dome is composed of a porphyritic, light grey-
377 coloured andesite (60.2 – 61.7 wt.% $SiO_2$) with plagioclase (13 vol. %), pyroxene (8
378 vol. %), and rare amphibole phenocrysts (4 vol. %). A K-Ar age obtained from a lava
379 sample from the summit (Loma de la Virgen) yielded an age of 138 ± 4 ka (COTA-
380 56; Table 1a). Importantly, this age agrees with the stratigraphic position of this unit,
381 which is almost contemporaneous with the main lava flow succession of Cotacachi
382 volcano basal member.

383

384 *Verde Tola unit ($Pl_{Up}$-VT & $Pl_{Md}$-VT)*

385 The olivine-rich Verde Tola lava flow succession (dark blue unit in Fig. 2), that forms
386 the Verde Tola hill at the lower north-eastern flank of Cotacachi, reaches between
387 3400 and 3900 m asl. This unit comprises a <100 m-thick lava flow succession, with
388 individual lava flows having a maximum runout of 2-3 km from the inferred emission
389 centre. Another < 30 m-thick lava flow succession crops out at the south-eastern
390 flank of the volcano, by the headwaters (3300 m asl) of the Alambi river valley (Fig.
391 2), where they concordantly overlay the Cotacachi basal lava flows, and reach 3 km
392 from the emission centre at the highest point of the Verde Tola hill. These lavas are
393 porphyritic, olivine-bearing basaltic andesites (54.7 - 55.9 wt.% $SiO_2$), with a mineral
394 assemblage of plagioclase (9 vol. %), clinopyroxene (3 vol. %), orthopyroxene (3 vol.
395 %), and olivine phenocrysts (4 vol. %). Two lava samples of the Verde Tola unit from
396 the SE and NE flanks were dated at 133 ± 9 (COTA-02) and 113 ± 6 ka (COTA-60,
397 Table 1a, Appendix figure C.1), respectively.

398

399 *Loma Negra dome unit ($Pl_{Up}$-LN)*

400 Loma Negra (3066 m asl) (red unit in Fig. 2, Fig. 4b) is an eroded lava dome located
401 at the eastern flank of Cotacachi volcano, with a basal surface of 1.9 $km^2$. It is
402 covered by a thick layer of reworked, well-compacted, black-coloured soil displaying
403 angular andesitic lithics. Loma Negra is composed of a porphyritic, light grey-

coloured andesite with plagioclase, amphibole, and scarce pyroxene phenocrysts. In addition, a matrix-supported mono-lithological breccia that includes the amphibole-bearing andesites (~20-30 vol.% of lithics) was identified at the eastern flank of Loma Negra dome (red hatched area in Fig. 2). This deposit has an estimated thickness of 10-20 m, reached 4-7 km from its inferred source, and covers a surface of 10-12 $km^2$. Given its stratigraphic position cutting the Cotacachi lavas on the SE flank, this dome appears to be younger than the lava flows of the southeastern flank of Cotacachi, which were dated at ~110 ka.

*Northwestern debris-avalanche deposit (NW DAD)*

This unit crops out 40 km along the Apuela river inside the Intag valley (yellow unit in Fig. 2), to the northwest and the southwest of the volcano. In the Intag valley, this deposit overlies part of the Western Cordillera basement formed by the Apuela quartz-diorite batholith (Boland et al., 2000). The NW-DAD has a maximum thickness of 60-70 m from the bottom of the river valley (COTA 40; at 35 km from the inferred source at north-western flanks of Cotacachi volcano, Appendix figure B) and forms conspicuous and isolated terraces along the valley (Fig. 6a, Appendix figure B). This deposit is a volcanic breccia characterized by blocky facies (approx. 30 vol.% of the deposit, e.g., individual lithics of basaltic andesites, andesites, and some red and black volcanic scoria, as well as different patches of debris flow deposits) with variable diameters from 0.5 to 1 m (4 m for the debris flow deposit patches), embedded in a fine light-grey well-compacted matrix. The mineralogy of andesite lithics found within this deposit is characterized by the ubiquitous presence of pyroxene. Interestingly, no amphibole-bearing andesites were identified in the NW DAD. Dense volcanic blocks display frequent jigsaw fractures. Mixed facies are also present and constitute the main percentage (60 vol.%) of the distal avalanche deposit. The deposit displays fine matrix injections and other small subrounded lithics incorporated from the Western Cordillera basement, in addition to a small number of lithics from the Apuela quartz-diorite batholith (less than 10 vol.%, ~0.25 m in diameter).

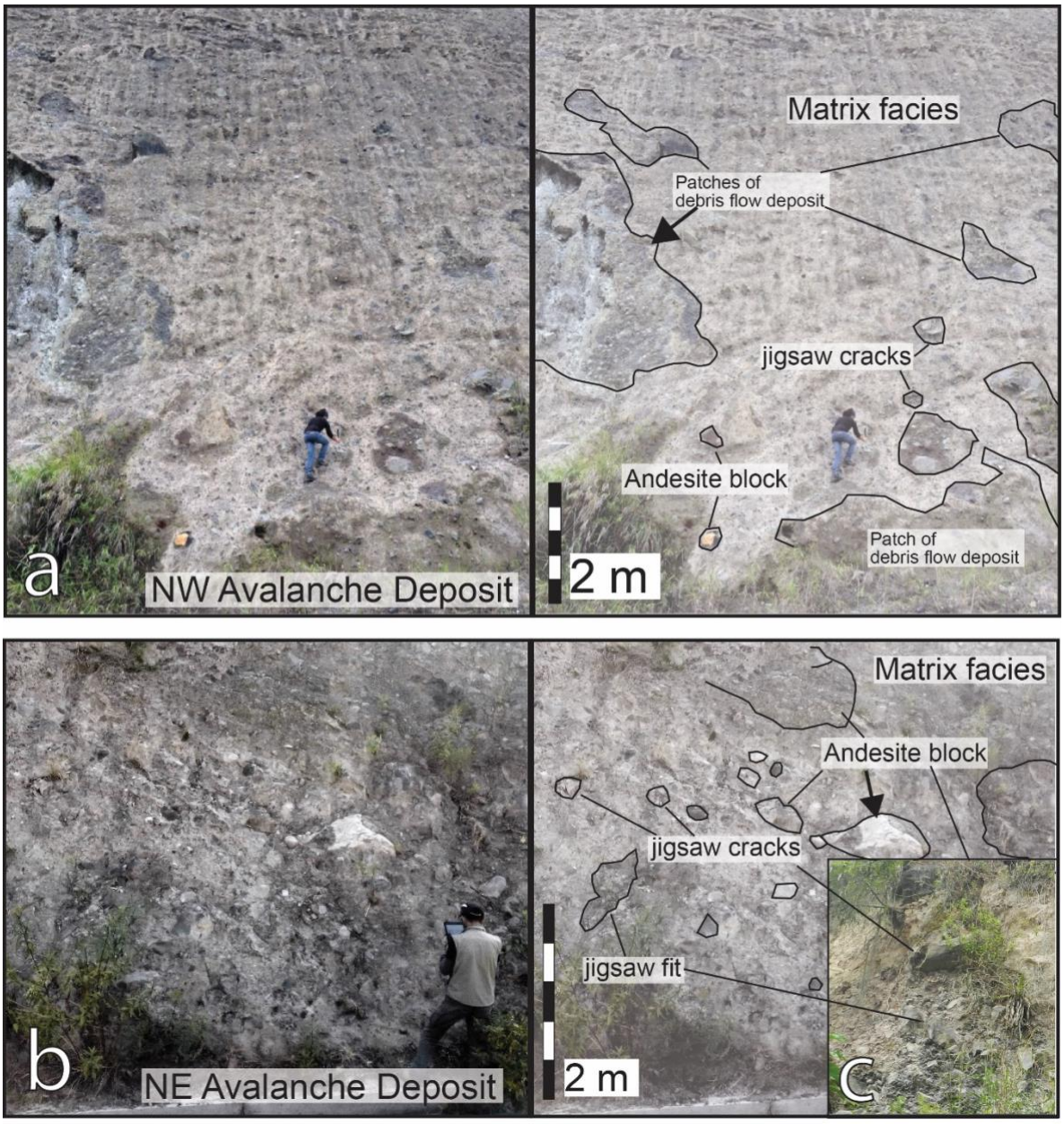


*Figure 6. Photographs of the (a) northwestern (Cota 40: 0.238046 N; 78.603827° W) and (b) northeastern (Cota 17: 0.398295° N; 78.135906° W) debris-avalanche deposits of the Cotacachi volcano. The northwestern deposit is located at the road that leads to the Intag valley, close to the Apuela town. The northeastern deposit is located at the Ambi river valley, close to the Imantag town. An interpretation of the deposits and their main structures is shown to the right. (c) First plane picture of the jigsaw – cracks and fit inside the NE avalanche deposit.*

444 ***Cotacachi Upper member***

445 *Upper lava flows ($Pl_{Up}$-Cot)*

446 The upper member of the Cotacachi edifice (orange unit in Fig. 2) comprises a steep
447 succession of lava flows (Figs. 3a and e). Access to these highly altered outcrops is
448 very difficult, allowing only limited sampling of the southern flanks over 4000 m asl,
449 on the ascent route to the summit. This lava flow succession reaches between 250
450 and 350 m thickness with a 1-2 km runout from the summit. This unit covers a surface
451 of 16 $km^2$ and includes some interlayered volcanic breccias. Also, the lava flows form
452 an angular unconformity over the basal lava flow succession ($Pl_{Md}$-Cot). This unit is
453 mainly formed by porphyritic andesites (59.8 – 60.7 wt.% $SiO_2$), which include some
454 andesitic enclaves. Some smaller (0.4 – 0.5 $km^2$) viscous lava flows on the hillside
455 (Fig. 3d) and summit (HO - LF; Fig. 3e) are part of this volcanic unit and are formed
456 by siliceous andesites (61.9 – 62.3 wt.% $SiO_2$) with a mineral assemblage of
457 plagioclase (14 vol. %), orthopyroxene (2 vol. %), clinopyroxene (4 vol. %), and some
458 scarce amphibole (2 vol. %) and olivine phenocrysts (< 1 vol. %). Sample COTA12
459 taken from this unit yields an age of 122 ± 8 ka (Table 1a and Appendix figure C.1),
460 which, within uncertainties, overlaps with the ages obtained from the top of the lava
461 succession of Basal Cotacachi I (110 ± 6 to 108 ± 6 ka).

462

463 *Northeastern debris-avalanche deposit (NE-DAD)*

464 This unit crops out at 30 km from the Cotacachi volcano, forming the terraces of the
465 Cari-Yacu and Ambi rivers (yellow unit in Fig. 2, Fig. 6b), along the north-eastern
466 flank of the edifice. The NE-DAD appears beneath the Piribuela dome pyroclastic
467 deposits (Appendices figures C.2 and B) and has a maximum thickness of 15-20 m
468 (Cota 17, Cota 38). The NE-DAD is a consolidated volcanic breccia that includes
469 block-rich facies (~25 vol.% of the deposit), which comprise debris flow deposit
470 patches and large blocks of pyroxene-bearing andesites (typical of basal member),
471 as well as a few amphibolic andesites and dacites (typical of the upper member).
472 Some blocks (mainly andesites), from ~ 0.25 to 2 meters in diameter, showing
473 frequent jigsaw fractures are also observed. This deposit has a fine-grained and
474 cohesive matrix (75 vol.% of the deposit) and incorporated rounded basement lithics

(~ 0.5 m in diameter). The mineralogy and geochemistry of the lava blocks in this avalanche deposit suggest that this event affected both basal and upper members of the Cotacachi cone.

Given that lava samples from the overlying Piribuela domes (presented below) yield an age of 65 ± 2 ka (Table 1a), and that the upper lava flows of the basal Cotacachi yielded ages of 108 ± 6 and 108 ± 4 ka (Table 1a), we propose that this debris-avalanche occurred between 108 ± 6 and 65 ± 2 ka. These ages agree with field observations, that the NE-DAD is distributed across the Ambi river valley, which was carved into the older Chachimbiro debris-avalanche deposit (dated between 405 ± 20 and 298 ± 32 ka; Bellver-Baca et al., 2019). In addition, long the right bank of Ambi river, the NE-DAD is overlain by the Imbabura debris-avalanche deposit (whose age is bracketed between 47 ± 6 and 30 ± 4 ka; Le Pennec et al., 2011; Andrade et al., 2019; Appendix figure C.2).

*Piribuela dome ($Pl_{Up}$-Pb)*

Piribuela dome (3871 m asl, 3.6 $km^2$) is located northeast of the Cotacachi summit volcano (red unit in Fig. 2, Fig. 4c). It is composed of porphyritic light grey and red-coloured dacites (63.6 – 64.8 wt.% $SiO_2$), which are the most differentiated eruptive products found at the CCVC (Fig. 10a, b, c). The mineral assemblage of Piribuela is composed of plagioclase (9 Avg. of Vol. %), amphibole (8 Avg. of Vol. %), biotite (altered crystals substituted by Fe-Ti oxides), and scarce pyroxene phenocrysts (1 Avg. of Vol. %). At least two mono-lithological, matrix-supported breccias, with a high percentage of dacitic lithics (~40 vol.%), were identified east-ward of the domes, overlying the NE-DAD at the Imantag to Piribuela road (red hatched area in Fig. 2, Appendix figure C.2), and interpreted as related to a young-looking scar present at the south-eastern flank of the dome (Fig. 4c). These deposits have an estimated thickness of 20-30 m, reaching 6-7 km from their inferred source, and covering a surface of 7-8 $km^2$. A sample of a dacitic juvenile block from this deposit yielded an age of 65 ± 2 ka (COTA26, Table 1a).

505 ***Cuicocha member***

506 *Pre-caldera unit (Ho-CuiD)*

507 The pre-caldera unit is composed of two sub-units, which correspond to the relicts
508 of the Cuicocha pre-caldera dome (red unit in Fig. 2, Fig. 4d), and some mono-
509 lithological volcanic breccias. Both are covered by a horizontal and compacted
510 deposit of orange-coloured fine-grained ash. This ash deposit shows a proximal
511 thickness of about 1 m decreasing to less than 5 cm at 16 km of distance.

512

513

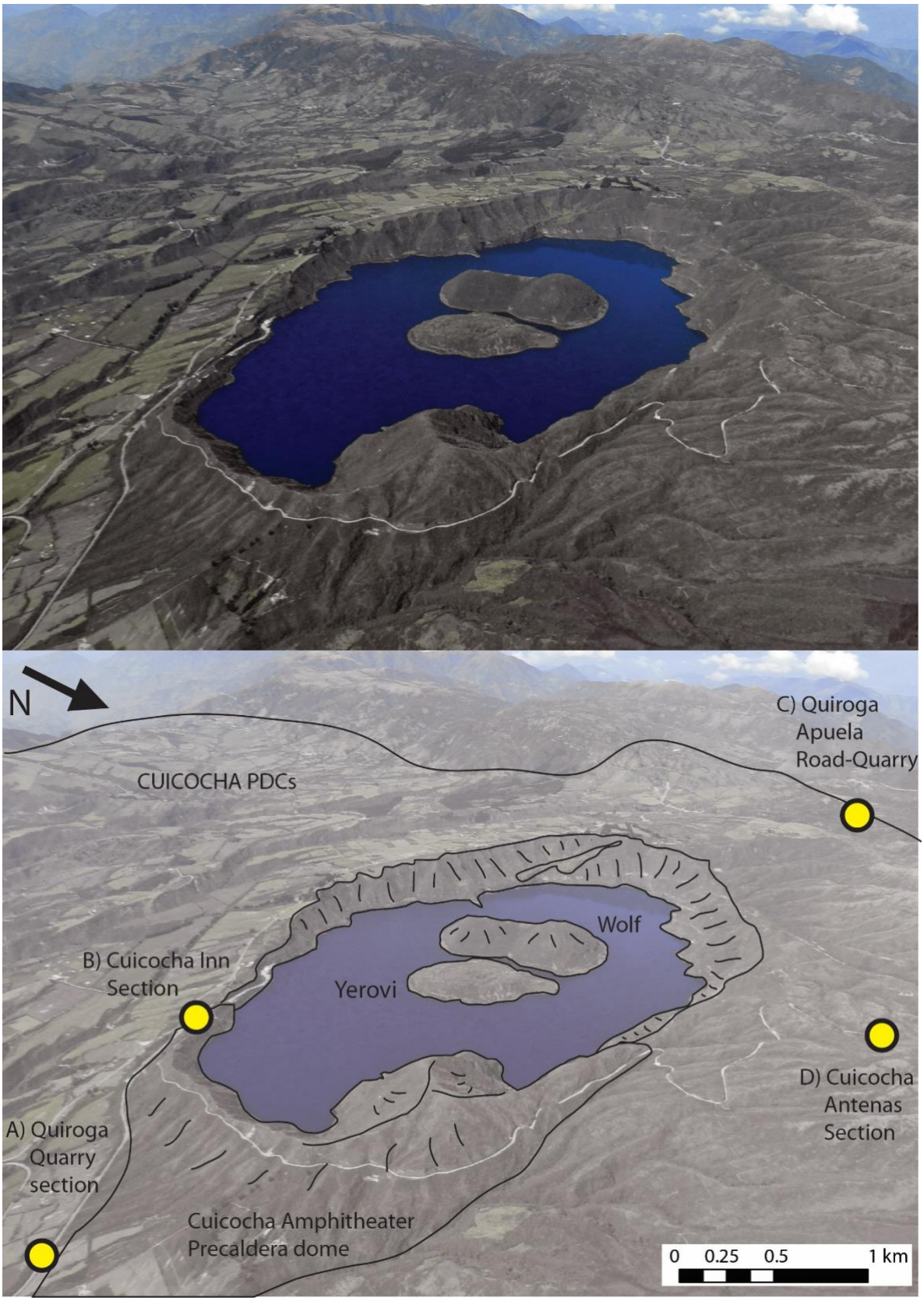
N
CUICOCHA PDCs
C) Quiroga
Apuela
Road-Quarry
Wolf
Yerovi
B) Cuicocha Inn
Section
D) Cuicocha
Antenas
Section
A) Quiroga
Quarry
section
Cuicocha Amphitheater
Precaldera dome
0 0.25 0.5 1 km

514

*Figure 7. Aerial photograph of the Cuicocha caldera. The remnants of the pre-caldera dome are observed, as well as the lake, the caldera rim, and the Wolf and Yerovi post-caldera domes. The yellow circles represent the location of stratigraphic sections presented in figure 8 and sampling points for radiocarbon ages (results are given in Table 1b).*

*Pre-caldera dome:* The most representative outcrops of the pre-caldera dome relicts were identified in the caldera lake inner north-eastern walls and outside the caldera (south-eastern flank) of Cuicocha, covering an estimated area of 1.7 $km^2$. Cuicocha dome also constitutes the highest point in the caldera border (3377 m). Cuicocha pre-caldera dome relicts display sub-vertical lava joints, which are light-grey siliceous andesites (58.1 - 62.8 wt.% $SiO_2$), with a mineral assemblage of plagioclase (14 vol. %) and amphibole (6 vol. %). Fe-Ti oxides are found replacing almost entirely some amphibole phenocryst. Occasionally, a small percentage of clinopyroxene (1 vol. %) is present in these rocks (Fig. 9). A sample of unaltered lava from the dome yielded a poorly defined K-Ar age due to its very small radiogenic argon ($^{40}Ar^{*}$) content (< 0.1%, Table 1a), but indicates that the dome was emplaced during Late Holocene times.

*Proximal monolithic breccia:* A relatively thin (1-2 m thick) layer of poorly sorted, matrix-supported breccia with a high percentage of dacite lithics (40-50 vol.%) and a dark-grey coloured, coarse-grained ash matrix covers the remnants of Cuicocha pre-caldera dome. This deposit is visible on the dome's southern flank, along the road that leads to the community of Apuela (1 km from the turn-off that leads to the entrance to the Cuicocha caldera lake, Fig. 8b), and at the inner walls of the southern caldera border.

At more distal outcrops (i.e., ~ 6 km westward along the same road), this matrix-supported breccia is observed to have a reduced percentage of porphyritic dacitic lithics (20-25 vol.%), as well as a dark grey to dark brown-coloured, medium-to-coarse-grained reworked ash matrix (< 2 mm size).

*Syn-caldera deposits (Ho-Cui)*

The syn-caldera deposit succession is composed of two volcaniclastic subunits that cover and smoothen the topography around Cuicocha lake (light green unit in Fig 2,

Fig. 8a). The syn-caldera deposit covers an area of 66.6 ± 0.1 $km^2$ and reaches as far as 13 - 15 km from the caldera lake towards the southeast (i.e., Hostería Cuicocha entrance, Quiroga quarries, between 3000 to 2500 m asl, Fig. 8c), and 3 - 4 km to the northwest (i.e., road from Cuicocha lodge to Muyurcu dome, between 3000 to 3300 m asl). Other thinner deposits were found to the north over the moorland (i.e., Las Antenas Road, between 3000 and 3900 m asl, Fig. 8d), reaching 3-4 km up the slope of the southern flank of Cotacachi.

The subunits are a basal and voluminous sequence of pumice-and-ash pyroclastic density current deposits overlain by a less-voluminous layer of surge deposits.

This syn-caldera pyroclastic succession overlays the pre-caldera units, and partially covers the southern flanks of the Cotacachi basal member (Fig. 8).

*Pyroclastic density current (PDC) deposits:* This subunit is a 5 to 40 m-thick (average of 20 m) succession of PDC deposits, formed by several pulses of caldera-forming explosive activity. In the field, each pulse can be identified by its pink-coloured top, which delimits PDCs horizons. At least 3 PDC layers are visible in the thickest outcrops such as Quiroga quarry, located 7 km to the south-east from the caldera lake. These deposits contain 30 vol. % of siliceous andesitic sub-angular pumice lapilli and blocks (61.8 – 62.7 wt. % $SiO_2$), supported in a matrix of light grey-coloured, medium-grained ash, which includes free plagioclase and hornblende crystals. Similarly, the pumice mineral assemblage is plagioclase (9 Avg. of Vol. %), amphibole (8 Avg. of Vol. %). In addition, dense lithics of Cuicocha pre-caldera dome were found to make up at least 5 vol. % of these PCD deposits.

*Surge deposits:* Several pyroclastic surge deposits (i.e., dilute pyroclastic current deposits) less than 1 m thick overlay the PDCs layers. They display a cross-bedded stratification, are poorly sorted and fine-grained containing < 3 cm-size pumice lapilli (and accretionary lapilli; Pidgen, 2014) and light-grey fine-grained ash. The juvenile lapilli-pumice clasts have a siliceous andesitic composition (62.1 – 62.4 wt. % $SiO_2$). Less than 3 vol. % of dense siliceous andesites from the pre-caldera dome composed of plagioclase, amphibole, and scarce biotite were also incorporated.

Different centimetre thick reworked volcaniclastic layers are interspersed within this succession between the pyroclastic flows and the pyroclastic surges, especially in

the moor area. Radiocarbon dating (Table 1b) of charcoal and soil samples found within Cuicocha syn-caldera deposits yields ages of 3525 ± 35 aBP (CUI-27B) at the base and 2980 ± 30 aBP (CUI-22B) at the top of the pyroclastic flows, which is concordant with the ages obtained by von Hillebrandt. (1989), of 2990 ± 300 a BP (Table. 1b).

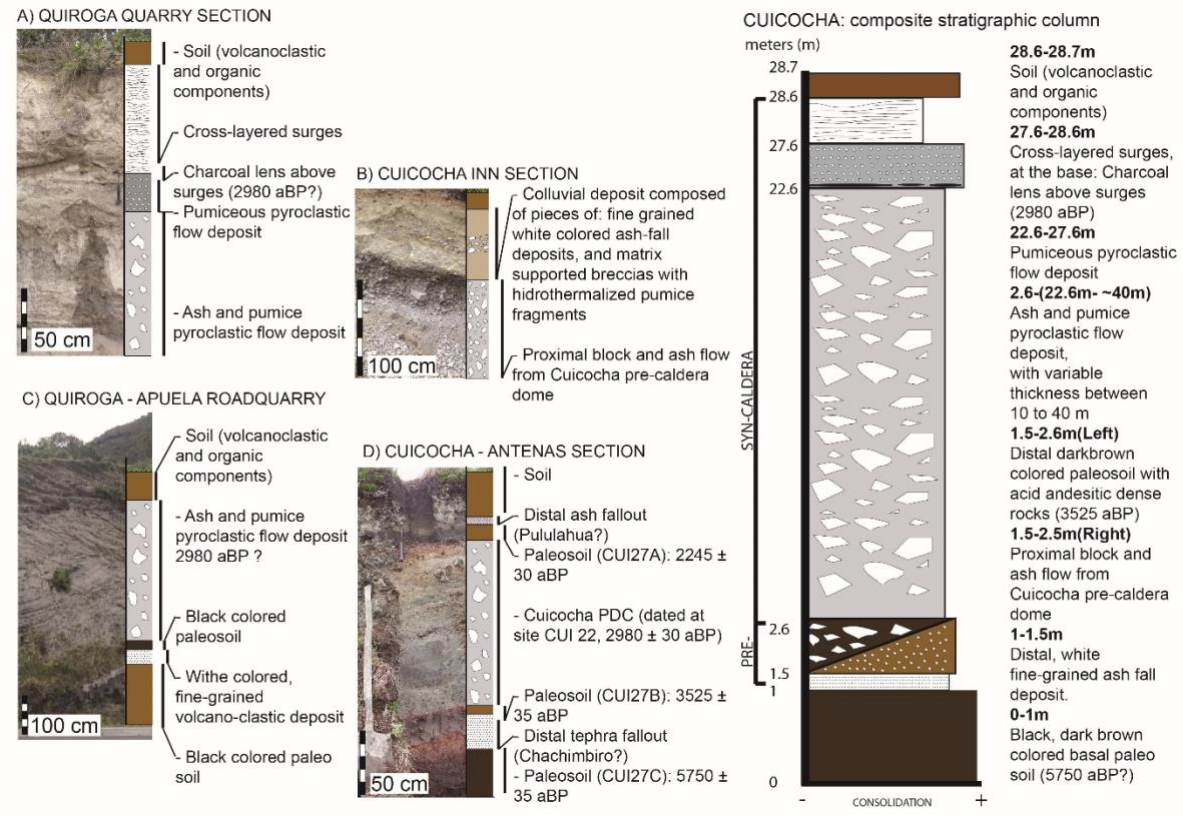


*Figure 8. A B, C, and D are different stratigraphic sections of Cuicocha Caldera. To the right: Composite stratigraphic column of the section of the Cuicocha member. Note the stratigraphy section's location at figure 7. All the dates here presented belongs to this study, see table 1b.*

*Post-caldera unit, Wolf and Yerovi domes (PC)*

This unit comprises four coalescent domes emplaced inside the Cuicocha caldera lake (Fig. 2, Appendix figure C.3), which form two volcanic islets called Wolf (maximum slopes of 48°) and Yerovi (maximum slopes of 35°, see section 4.1 for morphology and structure). The rocks that compose these domes are porphyritic siliceous andesites (61.5 – 62.2 wt.% $SiO_2$) bearing phenocryst of plagioclase (14 Avg. of Vol. %), amphibole (12 Avg. of Vol. %), inside a glassy matrix. These domes

were emplaced after caldera formation, which means that they are younger or coetaneous than 2980 ± 30 aBP (CUI-22B) (Table 1b).

### 4.4. Main petrographic and geochemical characteristics

The textures of the rocks that form the central edifice of Cotacachi are glomero-porphyritic to ophitic, with mostly euhedral shaped phenocrysts, while the rocks that form the domes and the products of Cuicocha Caldera are porphyritic with trachytic texture. In both cases, the matrix is constituted by glass and microlites of plagioclase (< 100 µm) and amphibole (for Cuicocha, Piribuela, and few in Muyurcu). Plagioclase constitutes the dominant crystals, present in a similar percentage (11 – 12 vol. %) in all stratigraphic members of the CCVC. On the contrary, the presence of olivine and amphibole crystals is not homogeneous. The amount of olivine in the rocks of the basal lava flows (2 vol. %) progressively decreases as the rocks become more silica-rich (Upper member), to fully disappear at Piribuela dome and Cuicocha member (Fig. 9, Appendix table B.1). The opposite is true for the amphibole phenocrysts, which progressively appear in the upper Cotacachi lava successions (4 vol.%), reaching a considerable content in the peripheral domes (Fig. 9), especially at Cuicocha (8 vol.%).

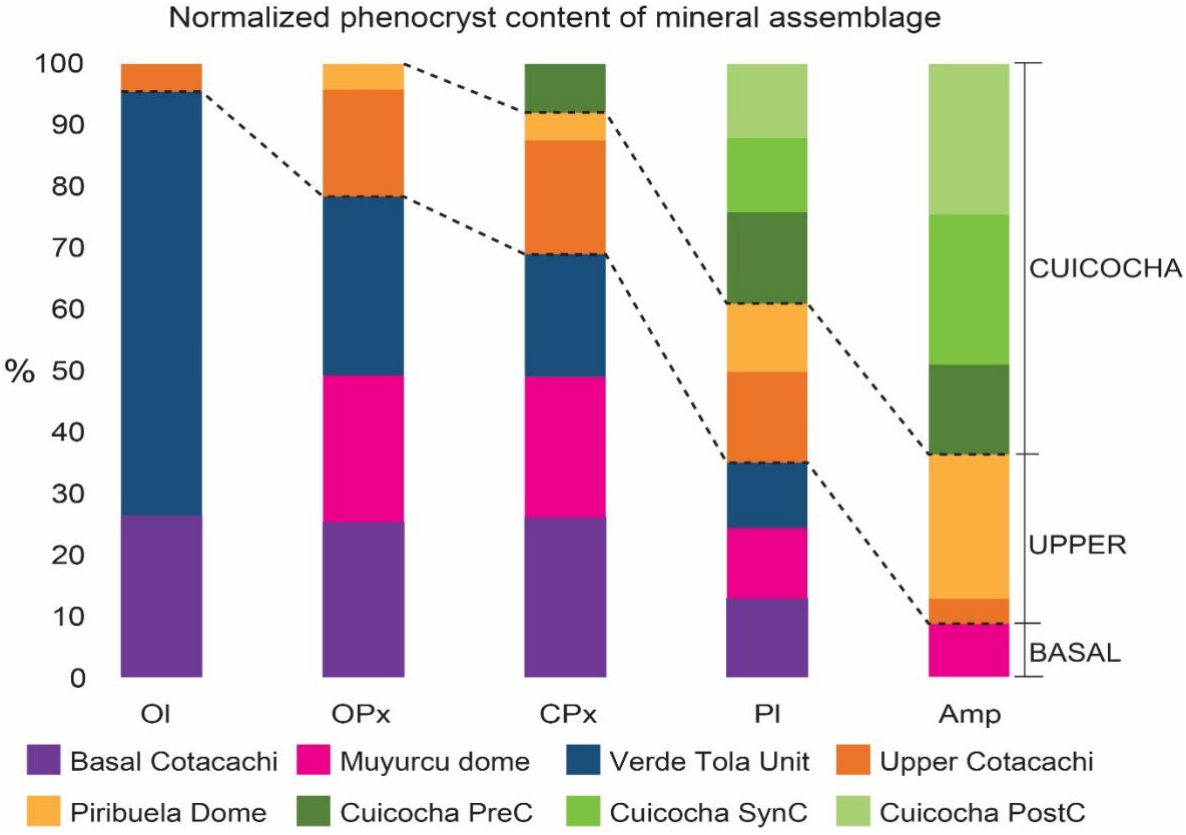


*Figure 9. Variability of Cotacachi - Cuicocha mineral assemblages in a base of a phenocryst normalization, see Appendix table B.1, note the transitional mineralogical change from Basal Cotacachi to Upper Cotacachi and Cuicocha member. Amp: amphibole, Pl: plagioclase, Cpx: clinopyroxene, Opx: orthopyroxene, Ol: olivine.*

CCVC rocks are calk-alkaline medium potassium basic to acidic andesites and dacites (54.68 – 64.83 wt.% $SiO_2$, 0.8 – 1.9 wt. % $K_2O$, Appendix table B.2) (Peccerillo and Taylor, 1976; Fig. 10a). They fall into the field of other erupted rocks produced in the Ecuadorian Western Cordillera (Hidalgo et al., 2012; Ancellin et al., 2017). In the primitive mantle normalized multi-elements diagram (Fig. 10b), all CCVC rocks display the Nb-negative anomaly and enrichments in Large Ion Lithophile Elements (LILE) as Rb, Ba, Th and K, typical of calc-alkaline rocks. A slight negative anomaly is also observed for P, while Heavy Rare Earth Elements (HREE) show mostly a flat pattern. Few samples from Cotacachi show a highly fractionated spectrum specially for Yb (Fig. 10b).

Major elements such as MgO, FeO, and CaO show negative correlations with silica, while $Na_2O$ and $K_2O$ show positive ones (Fig. 10c) as well as transition metals such

as Co, Ni, Cr, and Sc, show a compatible behaviour, illustrated by the Co *vs*. $SiO_2$ diagram in figure 10c. In contrast, the Light Rare Earth Elements (LREE, *e.g.,* Ce, La), and some Large Ion Lithophile Elements (LILE, e.g., Rb, Ba), show incompatible behaviour, illustrated by the Rb *vs*. $SiO_2$ diagram (Fig. 10c). Th, Rb, La, and Ba in Cuicocha rocks follow the same pattern as $K_2O$.

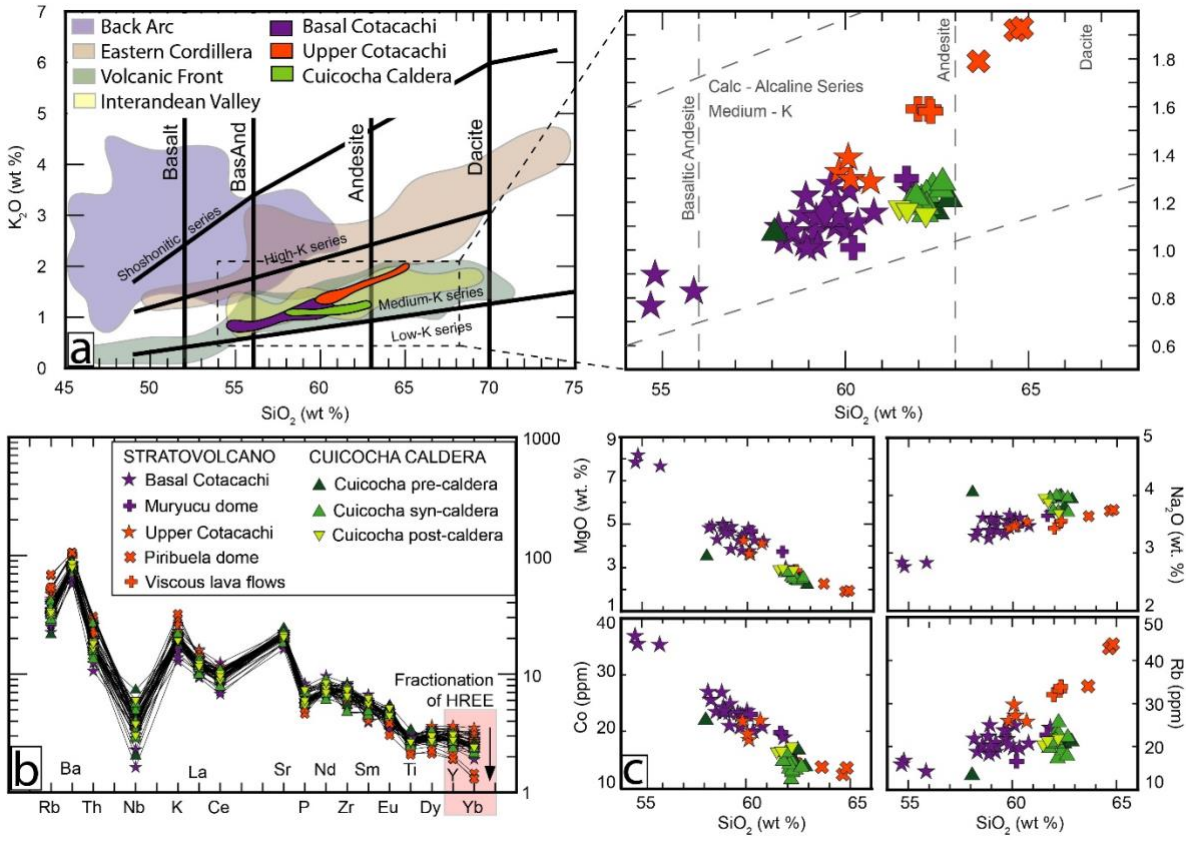


*Figure 10. a) Left: $K_2O$ vs. $SiO_2$ diagram from Peccerillo and Taylor (1976) for representative samples of the Ecuadorian Volcanic Arc (modified from Hidalgo et al., 2012). The CCVC samples are highlighted. Right: Zoom to CCVC $K_2O$ vs. $SiO_2$ members and units. b) Diagram of trace element content of CCVC rocks normalized to the primitive mantle (Sun and McDonough, 1989), note the high fractionation of the HREE (e.g., Yb) highlighted in the red-colored square. c) Representative Harker diagrams (MgO, $Na_2O$, Co and Rb) of CCVC members and units.*

## 4.5. Bulk volumes and eruptive rates

*Bulk volumes*

Results obtained using the interpolation MatLab script (see Andrade et al., 2021) with input surface values of 107 ± 3 $km^2$ and heights ranging between 2519 and 4939 m asl, yield an estimated minimum bulk volume of 56 ± 4 $km^3$ for all CCVC proximal eruptive products currently remaining (i.e., the non-eroded volume; Fig. 11), where the ± 4$km^3$ represent the standard deviation of the analytical results. However, to reduce the uncertainty of this method we must consider an error of ± 2% in the cartographic boundary used by the script, which can modify the resulting volume by up to ± 10 – 20 %. Applying the ShapeVolc reconstruction method (Lahitte et al. 2012), we calculated a minimum bulk volume of emitted material of 91 ± 25 $km^3$ for the end of the CVCCs main construction stage (approx. 100 ka). The difference between the current (56 ± 4 $km^3$) and the reconstructed volume (91 ± 25 $km^3$) is 36 ± 9 $km^3$, which represents the eroded volume since the end of the construction of the Upper Cotacachi, i.e., during the last 100 ka, which defines an erosion rate of 0.3 ± 0.1 $km^3$/kyr (Table 2b). We can assume a similar average erosion rate for both periods, since the syn-construction and post-construction periods (i.e., 173 ± 4 to 108 ± 6 ka, and after 108 ± 6 ka, respectively) both experienced a full glacial-interglacial cycle, and the average volume of the volcanic complex during these two stages is comparable. Therefore, applying the post-construction erosion rate of 0.3 ± 0.1 $km^3$/kyr to the syn-construction period of the basal and Upper Cotacachi members, the volume eroded between 173 ± 4 and 108 ± 6 ka is estimated at 21 ± 6 $km^3$. Finally, by adding this syn-construction eroded volume to that reached by the volcano at the end of its construction stage (91 ± 25 $km^3$), we obtain a total erupted volume of 112 ± 31 $km^3$ for the uneroded Cotacachi basal and upper edifices (100ka stage, Fig. 11b).

a

| Unit | Surface ($km^2$) | Extrapolated max. Volume ($km^2$) | Estimated minimum bulk Volume ($km^3$) | Estimated Volume ($km^3$) | Estimated Volume thick (m) | Estimated Volume thick (m) | Estimated average thick (m) | Maximum lenght (m) |
|---|---|---|---|---|---|---|---|---|
| Basal Cotacachi | 107.3 | | 49 ± 4 | | | | | |
| NW DAD | 12 | 63 | 0.5 ± 0.2 | 1.1 ± 0.1 | 66 | 24 | 45 | 40 |
| Muyurcu dome | 2.4 | | 0.3 | | | | | |
| Loma Negra dome | 1.9 | | 0.1 | | | | | |

| | | | | | | | | | |
|---|---|---|---|---|---|---|---|---|---|
| | Upper Cotacachi | 16.2 | | 1.7 | | | | | |
| | NE DAD | 12 | 41 | 0.2 ± 0.1 | 1.8 ± 0.5 | 20 | 16 | 18 | 30 |
| | Piribuela dome | 3.6 | | 0.3 | | | | | |
| | Cuicocha pre-caldera | 1.6 | | 0.1 | | Cuicocha total Volume ($km^3$) | 56 ± 4 | Cuicocha total volume ($km^3$) | 4.2 ± 0.1 |
| | Cuicocha syn-caldera | 66.6 | | 4.1 | | | | | |
| | Cuicocha post-caldera | 0.8 | | 0.04 | | | | | |

b

| Stage | Age max. | Age min. | Period | Raw volume | Eroded volume | Total, volume | Eruptive rate | | Erosion rate | |
|---|---|---|---|---|---|---|---|---|---|---|
| | ka | ka | ka | $km^3$ | $km^3$ | $km^3$ | $km^3$/kyr | mm/yr | $km^3$/kyr | mm/yr |
| Construction Basal + Upper Cotacachi | 173 ± 4 | 108 ± 6 | 65 ± 7 | 91 ± 25 | 21 ± 6 | 112 ± 31 | 1.7 ± 0.5 | 7.4 ± 2.2 | | |
| Erosion since the end of Upper cotacachi construction | 108 ± 6 | 0 | 108 ± 6 | | | 36 ± 9 | | | 0.3 ± 0.1 | 1.4 ± 0.4 |

*Table 2. a) Volume estimations in base of a MatLab interpolation using the 4m resolution digital elevation model (Instituto Geográfico Militar - IGM). b) Result of volumes, eruptive and erosion rates calculations obtained from ShapeVolc software (Lahitte et al., 2012) and given at 1-sigma accuracy.*

Due to the high erosion rate, the NW and NE debris-avalanche deposits are found scattered in form of isolated terraces in the Intag and Ambi river valleys (Appendix figure B), respectively. In addition, the traces of the supposed corresponding scars in the higher flanks have been strongly eroded, impeding any avalanche volume calculations based on the scar sizes (Appendix figure B). Therefore, minimum volumes were calculated for the currently observed remaining debris-avalanche deposit terraces, while maximum volumes were estimated by extrapolating the potentially eroded deposit surface and using average thickness values of 45 and 18 m for the NW- and NE-DAD, respectively. In this manner, for the NW-DAD, which is found between 3282 and 1960 m asl, we obtained volumes between 0.5 ± 0.2 $km^3$ and 1.8 ± 0.5 $km^3$, covering a surface of 12 to 41 $km^2$, respectively. For the NE-DAD, found between 2315 to 1637 m asl, the estimated volumes range from 0.2 ± 0.1 $km^3$ to 1.1 ± 0.1 $km^3$, covering surfaces of 12 to 63 $km^2$, respectively.

For Cuicocha deposits, a current bulk volume of 4.2 ± 0.1 $km^3$ was obtained using the MatLab interpolation script including the pre-, syn- and post-caldera deposits, which cover a surface of 68 $km^2$, with a variable altitude from 2535 to 3910 m asl.

This volume value agrees with the minimum volume of 4.1 $km^3$ estimated by von Hillebrandt (1989). In addition, tephra fallout deposits of Cuicocha cover a surface of approximately 6.8 x $10^2$ $km^2$, reaching the northern Ecuadorian coastline 176 km away from the volcano. A volume estimation based on the Legros (2000) method for a single isopach, results in 2 $km^3$ of tephra fallout, using a representative thickness of 0.08 m (calculation detailed in Vallejo Vargas, 2011).

*Eruptive rates*

A minimum bulk emission rate of 1.7 ± 0.5 $km^3$/ka for the main basal Cotacachi lava flows, was obtained using the step times of 65 ka (Cotacachi stratovolcano).

If we include the last age (2.98 ka) corresponding to the Cuicocha eruption (4.2 $km^3$), we obtain an emission rate of 0.068 ± 0.016 $km^3$/ka (pause time of 62 ka, since the formation of the Piribuela dome until the Cuicocha pre-caldera dome development), corresponding to this last period of CCVC construction. Such drop in Cotacachi volcano bulk emission rate from 1.7 ± 0.5 to 0.068 ± 0.016 $km^3$/ka indicates a progressive decrease in its eruptive activity.

## 5. DISCUSSION

### 5.1. Chronological evolution of CCVC

According to the chronology obtained during this study, the eruptive activity of the CCVC suggest this volcanic centre is among the youngest of the Western Cordillera of the Ecuadorian Andes. Indeed, the Cotacachi stratovolcano (173 ± 4 to approx. 15 ka; this study, Fig. 11a) is younger than Cushnirumi (411 ± 8 to 383 ± 6 ka; Bablon et al., 2020), Mojanda (1038 ± 87 to 194 ± 6 ka; Bablon et al., 2020) and Cusin (517 ± 8 to 495 ± 12 ka; Bablon et al., 2020). It is contemporary to the development of Fuya Fuya (476 ± 38 to 28 ± 5 ka; Bablon et al., 2020), Chachimbiro (approx. 405 to 5 ka; Bernard et al., 2014, Bellver-Baca et al., 2019, Bablon et al., 2020), Cubilche (45 ± 5 to 40 ± 5 ka; Navarrete et al., 2020, Bablon et al., 2020), and Imbabura (47 ± 6 to approx. 8 ka; Le Pennec et al., 2011, Andrade et al., 2019, Bablon et al., 2020). Finally, the Cuicocha (3525 ± 35 aBP to 2980 ± 30 aBP) explosive volcanism is one of the youngest in the northern part of the Ecuadorian Andes together with

728 Pululahua Dome Complex dated at approx. 2600-2300 aBP (Andrade et al, 2021;
729 Vásconez Müller et al., 2022).

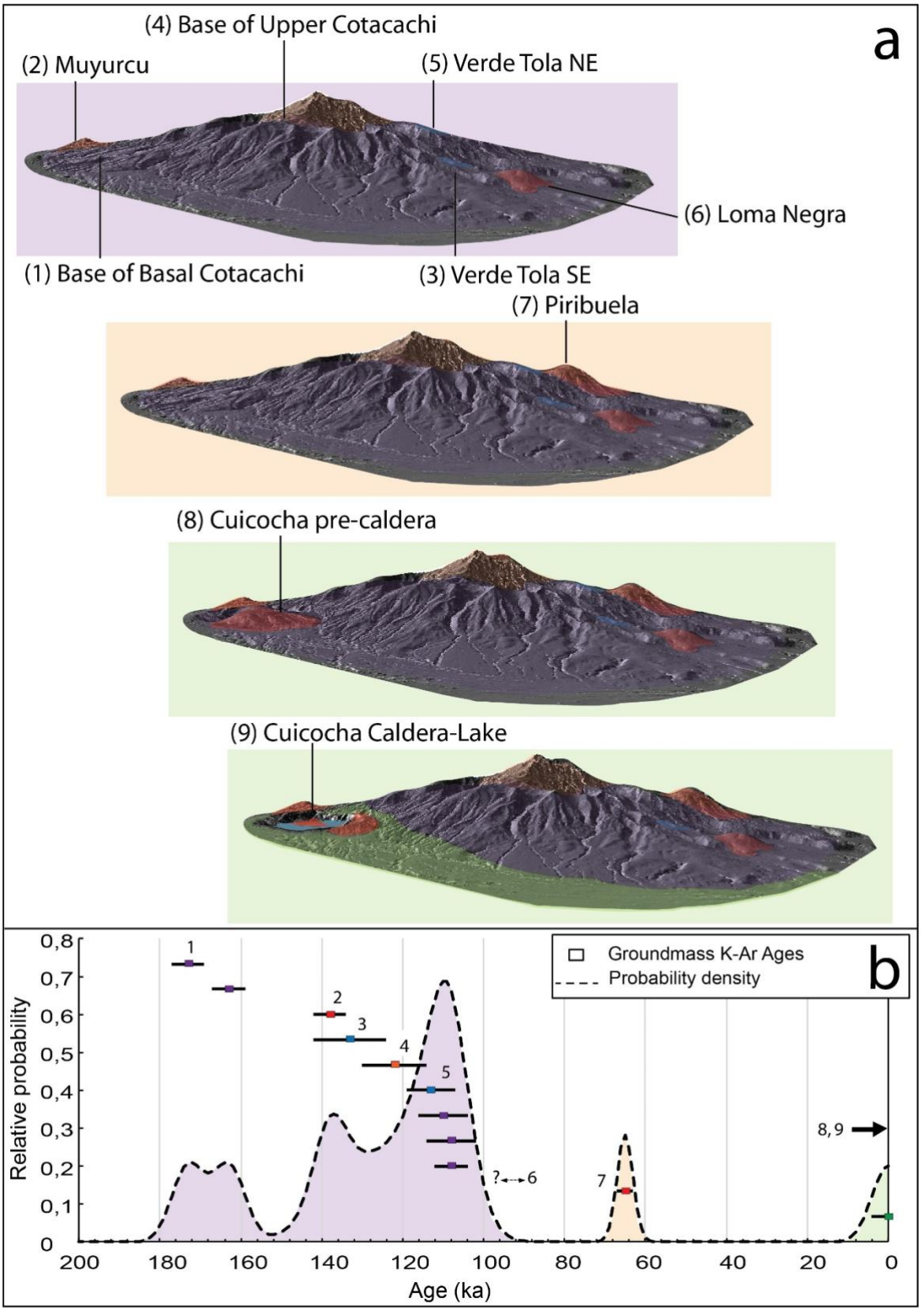
a
(4) Base of Upper Cotacachi
(2) Muyurcu
(5) Verde Tola NE
(6) Loma Negra
(1) Base of Basal Cotacachi
(3) Verde Tola SE
(7) Piribuela
(8) Cuicocha pre-caldera
(9) Cuicocha Caldera-Lake
b
Groundmass K-Ar Ages
Probability density
Relative probability
0,8
0,7
0,6
0,5
0,4
0,3
0,2
0,1
0
1
2
3
4
5
?↔6
7
8,9
200
180
160
140
120
100
80
60
40
20
0
Age (ka)

730

*Figure 11. a) Morphological and chronological reconstruction of Cotacachi-Cuicocha Volcanic Complex. b) Gaussian Age-probability spectrum (calculation detailed in Deino and Potts, 1992), outlining potential gaps of activity between 100 and 65 ka, and between 65 and ~4 ka. Groundmass K-Ar ages are shown with the same color used for units from figure 2.*

*Cotacachi strato-volcano*

The age probability curve (Fig. 11b) calculated from the K-Ar ages obtained here for the volcanic complex shows six peaks of activity, with three growth gaps. It highlights the formation of the basal stratovolcano (Cotacachi) between 180 and 100 ka. Within this interval, the first short hiatus of activity is followed by the extrusion of the southwest Muyurcu dome and the subsequent emission of lavas from the Verde Tola unit (SE: 133 ka and NE: 113 ka). The younger construction phase of the Cotacachi strato-volcano occurred between 122 and 108 ka. The following two stages of activity (70 to 60 ka, and less than 10 ka, respectively) are associated with the extrusion of the Piribuela (the most silica-rich dome of CCVC; dated at 65 ka) and Cuicocha domes. Nevertheless, we must keep in mind that such age-probability curve is biased by the low number of available ages, mostly due to the lack of sample from difficult-to-access units (e.g., summit lava flows). Note that the plagioclase (CUI-30A) age of 207 ± 25 ka is much older than the age obtained from the groundmass of the same sample (Table 1a). This suggests that, as observed elsewhere (e.g., Singer et al., 1998), plagioclase crystals could have been incorporated in the magma reservoir and did not have time to be reset before the eruption. This led to an apparent K-Ar age older than the age of the eruption. This example supports the importance of carrying K-Ar ages on groundmass for young volcanic material.

The main cone-building stage (Middle to Upper Pleistocene, starting at 173 ± 4 ka) of the Cotacachi cone is represented by the emission of a thick succession of andesitic lava flows, which form the lower and middle flanks of the edifice, constructed directly over the Cretaceous to Paleocene basement of the Western Cordillera. Some peripheral domes were formed subsequently, starting with the oldest south-western Muyurcu, at about 140 ka. Stratigraphic relationships show that the south-eastern Loma Negra dome is younger than 108 ± 6 ka. During the period between 140 and 108 ka, the lava flows of Verde Tola were emitted, the composition (54.7 - 55.9 wt.% $SiO_2$) of which suggests an apparent effusive type of activity,

764 forming two isolated (SE: 133 ± 9 ka, NE: 113 ± 6 ka) olivine-bearing and
765 magnesium-rich basaltic-andesitic lava flow successions. A 5 km large amphitheatre
766 that opens to the NW cuts the basal lava flows of Cotacachi. The corresponding
767 debris avalanche deposits reach approx. 40 km along the Intag valley and are
768 characterized by the absence of amphibole-bearing andesites, which is typical for
769 the Upper Cotacachi member. Based on the description we suggest this first north-
770 western debris avalanche occurred before 108 ± 6 ka.
771 The upper and steep flanks of the Cotacachi stratocone represent the last phase of
772 development of the main cone-building stage (Cotacachi upper member). The
773 youngest ages of the Basal member (110 ± 6 and 108 ± 6 ka), overlap the oldest
774 age (122 ± 8 ka) of the Upper lava flow succession (Appendix figure C.1), which can
775 be interpreted as the loss of the youngest section of this building stage, due to the
776 intense erosion rate we have obtained here (0.3 ± 0.1 $km^3$/kyr). The second partial
777 flank collapse event occurred on the north-eastern flank, leaving a debris avalanche
778 (NE-DAD) deposit that crops out towards the Ambi river valley and is covered by the
779 Piribuela deposits at the proximal facies and by the Imbabura DAD at its distal facies
780 (Appendix figure C.2). Interaction between the avalanche and the glacier has had an
781 important implication in the fluidization of the moving mass (Deline, 2009) of the NE-
782 DAD, giving the deposit an appearance of a big lahar. Since Piribuela dome was not
783 affected by the debris avalanche event and its associated deposits overlay the NE
784 avalanche, the NE-DAD must have taken place between 108 ± 6 and 65 ± 2 ka.
785 Following the discrimination between volcanic debris and rock avalanches (Dufresne
786 et al., 2021), we have tried to establish the origin of those observed at CCVC. Due
787 to the low juvenile clast content as well as the apparent structural control provided
788 by the Billecocha fault system, we propose that the debris avalanche events at
789 CCVC originated from tectonic disturbances rather than from violent eruptions. The
790 last evidence of eruptive activity of Cotacachi edifice corresponds to the summit lava
791 flows (Fig. 4e, Fig. 5a), which lack glacial erosion, suggesting an age younger than
792 the LGM (i.e., from 33 to 14 ka; Clapperton, 1990; Samaniego et al., 2012; Bablon
793 et al., 2019). In addition, Ego et al. (1996) suggests a specific period of activity for
794 the Billecocha fault system between 5.7 and 10 ka BP. Considering that the summit

lava flows have not been affected by the regional tectonics, Cotacachi activity could have lasted until 15 - 10 ka BP. Cuicocha pre-caldera dome ($^{14}C$: 5750 ± 35 aBP to 3525 ± 35 aBP; Table. 2b), is the youngest volcanic dome in the evolution of the CCVC, whose destruction resulted in the formation of the Cuicocha caldera lake.

*Cuicocha explosive event*

The caldera-forming eruption of Cuicocha is characterized by a large succession of pyroclastic density currents (i.e., pumice and ash pyroclastic flows, and surges) that covers a large surface (67 $km^3$, Table 2a) around the caldera (von Hillebrandt, 1989; Pidgen, 2014; Fig. 2, Fig. 7).

This explosive phase (Syn-caldera unit) is related to the destruction of the pre-caldera Cuicocha dome and the formation of the first crater/depression. Successions of poorly stratified pyroclastic-flow deposits are related to the paroxysmal phase of the eruption (Pidgen, 2014). Additionally, the physical characteristics of Cuicocha surge deposits (i.e., highly fragmented, fine-grained deposits, presence of accretionary lapilli, and cross/layered stratification) reveal that an intense phreatomagmatic activity took place during a new dome construction phase in a subaqueous environment (i.e., inside the first caldera lake) ($^{14}C$: 2980 ± 30 aBP). The Cuicocha eruption ended with the formation of the Wolf and Yerovi post-caldera domes (von Hillebrandt, 1989; Pidgen, 2014). The volumes of 4.2 ± 0.1 $km^3$ and ~2 $km^3$ obtained for the proximal PDC deposits and tephra fallout deposits, respectively, classify this event with a Volcanic Explosivity Index of 5 (VEI= 5; Newhall and Self, 1982). Our data suggest that the pre-caldera lava dome formation, the syn-caldera explosive phase, and the post-caldera dome growth of Cuicocha, occurred during a period spanning roughly 1.5 ka, probably involving more than one eruptive event. The resulting morphology produced by the above-described phenomena is a funnel-shaped caldera, which main characteristic is their shape, resulting from the outward widening of the vent, through erosive and gravitational mechanisms, such as progressive subsidence of a highly fractured crater (Lipman, 2000; Cole et al., 2005). Future work should address the formation of the observed Cuicocha depression in more detail since the present interpretations are based on its morphology.

826

827 ## 5.2. Contextualizing volumes, erosion, and eruptive rates

828 The erupted volume corresponds to the difference between the basement elevation
829 interpolation and the elevation model at the end of CCVC construction, while the
830 post-construction eroded volume corresponds to the difference between the
831 elevation model at the end of edifice construction and the present-day morphology.
832 As detailed in Bablon et al. (2018), eruptive rates were calculated using durations
833 derived from age differences between the beginning and the end of the main
834 construction stages, whereas post-activity erosion rate calculations involved the time
835 elapsed since the end of Cotacachi construction. Then, although both methods have
836 allowed estimating volumes, their limitation lies in the quantification of the cause-
837 effect produced by loss of data (Andrade et al., 2021; Vásconez Müller et al., 2022).
838 In this sense, estimated volume should be considered with caution and are
839 presented with a high uncertainty due to biases that can be induced by erosion (loss
840 of data from younger sequences), modelling of the basement elevation, as well as
841 the possible flank collapses.
842
843 By comparing the bulk volume results obtained for the current and the reconstructed
844 Cotacachi-Cuicocha Volcanic Complex (56 vs. 91 $km^3$) with those of other andesitic
845 - dacitic volcanic complexes in the Ecuadorian arc (Pichincha volcanic complex: 30
846 to 250 $km^3$, Robin et al., 2010; Chimborazo: 63 to 100 $km^3$, Samaniego et al., 2012;
847 Imbabura: ~ 65 $km^3$, Cushnirumi: ~53 $km^3$, Bablon et al., 2020) and others with
848 similar characteristics in the Andes (Ampato Sabancaya – Peru: 44 - 54 $km^3$,
849 Samaniego et al., 2016; El Misti – Peru: 70 $km^3$, Thouret et al., 2001), we observe
850 that the CCVC is among the more voluminous volcanoes of the Northern and Central
851 Volcanic Zones of the Andes.
852 In contrast, the range of volumes obtained for the NW (0.5 – 1.8 $km^3$) and NE (0.2 –
853 1.1 $km^3$) avalanches are smaller than other Ecuadorian avalanche deposits (i.e.,
854 Sangay: ~33 $km^3$, Valverde et al., 2021; Chimborazo: 10 – 12 $km^3$, Samaniego et
855 al., 2012; Tungurahua: 8 $km^3$, Hall et al., 1999; Cubilche: 3 $km^3$, Roverato et al.,

2018), as well as others from continental volcanoes (i.e., Saint Helens-USA: 2.5 $km^3$, Voight et al., 1981; Oshima – Japan: 2.5 $km^3$, Satake and Kate, 2001).

Moreover, we estimated that 36 ± 9 $km^3$ of material have been eroded since the end of Cotacachi construction (~100 ka), corresponding to an average erosion rate of 0.3 ± 0.1 $km^3$/kyr. This erosion rate is one of the highest obtained in the Ecuadorian Andes, only comparable to those of Carihuairazo volcano (Samaniego et al., 2022), South Iliniza volcano (Santamaria et al., 2022) and the oldest stage of Tungurahua volcano (~0.2 ± 0.1 $km^3$/kyr; Bablon et al. 2020). The high erosion rates in CCVC can be related to the combination of tectonic events with common erosion processes (such as glacial, fluvial and wind erosion) during its evolution.

Finally, the decrease observed for the CCVC's bulk emission rate, from 1.7 ± 0.5 for Cotacachi to 0.068 ± 0.016 $km^3$/ka for Cuicocha, is similar to the case of Chimborazo volcano, which declines from 1.6 to 0.3 $km^3$/ka, from the basal to the youngest cone, respectively (Samaniego et al., 2012).

## 6. CONCLUSIONS

The Cotacachi-Cuicocha Volcanic Complex (0.361° N; 78.349° W) is composed of a stratovolcano (Cotacachi: 173 ± 4 until the end of the Pleistocene), four peripheral/satellite domes (Muyurcu: 138 ± 4 ka; Loma Negra: younger than 108 ka; Piribuela: 65 ± 2 ka and Cuicocha pre-caldera: about 3 ka), and a funnel-shaped caldera, currently occupied by a lake, formed during a large explosive event dated at 2980 ± 30 a BP (4.2 ± 0.1 $km^3$ of emitted material) that ended with the extrusion of two post-caldera domes. Cuicocha is considered a potentially active volcano that is currently monitored.

CCVC rocks ranges from basic to siliceous andesites and dacites (54.7 – 64.8 wt.% $SiO_2$), whose chemistry corresponds to medium potassium, calc-alkaline magmatic series and exhibits the typical trend of the rocks erupted at the Western Cordillera

887 and Inter-Andean Valley of the Ecuadorian Andes (Hidalgo, et al., 2012; Fig. 10).
888 Cuicocha siliceous-andesites are slightly depleted in $K_2O$ and some trace elements
889 such as Th, Rb, La, and Ba, displaying a different trend to that of Cotacachi
890 stratovolcano and its peripheral domes. The mineral assemblage of the stratigraphic
891 members (Basal and Upper Cotacachi, and Cuicocha) of CCVC shows a
892 characteristic transition defined by the progressive disappearance of olivine and the
893 appearance of amphibole and biotite as silica content increases.
894
895 The CCVC, is one of the youngest (Middle Pleistocene to Holocene), and largest
896 (4939 m asl; 56 to 91 $km^3$ bulk volume) volcanoes in the northern Western Cordillera
897 of Ecuadorian Andes. Due to its height, its high elevation, and its proximity to active
898 faults, it has suffered a strong erosion (~0.3 $km^3$/kyr), that should be linked to fluvial,
899 wind, glacial, and tectonic processes. This erosion rate is among the most important
900 of the entire Ecuadorian arc.
901
902 In addition, two small avalanches affected different volcano flanks (NW, along Intag
903 valley, and NE, along Ambi river valley flanks, respectively) at different stages of its
904 formation. The north-western avalanche (0.5 ± 0.2 to 1.8 ± 0.5 $km^3$; older than 108
905 ka) affected the Basal edifice, and the north-eastern avalanche (0.2 ± 0.1 to 1.1 ±
906 0.1 $km^3$; 108 – 65 ka) affected the Upper lava flow succession.
907
908 **7. ACKNOWLEDGEMENT**
909 The results presented in this work are the result of a long-lasting Ecuadorian French
910 cooperation program, carried out between the Instituto Geofísico de la Escuela
911 Politécnica Nacional (IG-EPN) through SENPLADES project (Generación de
912 Capacidades para la Emisión de Alertas Tempranas), and the Institut de Recherche
913 pour le Développement (IRD, France) through a “Laboratoire Mixte International”
914 program entitled “Séismes et Volcans dans les Andes du Nord”. We deeply thank
915 the anonymous reviewers and the Invited Editor, C. Vallejo, for their insightful
916 comments that improve the manuscript.
917

## 8. REFERENCES


Alvarado, A., Audin, L., Nocquet, J. M., Jaillard, E., Mothes, P., Jarrín, P., Cisneros, D., 2016. Partitioning of oblique convergence in the Northern Andes subduction zone: Migration history and the present-day boundary of the North Andean Sliver in Ecuador. *Tectonics, 35(5)*, 1048-1065.

Ancellin, M. A., Samaniego, P., Vlastélic, I., Nauret, F., Gannoun, A., Hidalgo, S., 2017. Across-arc versus along-arc Sr-Nd-Pb isotope variations in the E Ecuadorian volcanic arc. *Geochemistry, Geophysics, Geosystems*, *18*(3), 1163-1188.

Andrade, S. D., van Wyk de Vries, B., & Robin, C., 2019. Imbabura volcano (Ecuador): The influence of dipping-substrata on the structural development of composite volcanoes during strike-slip faulting. *Journal of Volcanology and Geothermal Research*, *385*, 68-80.

Andrade, S. D., Müller, A. V., Vasconez, F. J., Beate, B., Aguilar, J., Santamaría, S., 2021. Pululahua dome complex, Ecuador: eruptive history, total magma output and potential hazards. *Journal of South American Earth Sciences*, *106*, 103046.

Bablon, M., 2018. Reconstruction de l'histoire des volcans de l'arc équatorien: contraintes pour l'évolution chronologique de l'arc andin et pour l'évaluation du risque volcanique (Doctoral dissertation, Paris Saclay).

Bablon, M., Quidelleur, X., Samaniego, P., Le Pennec, J. L., Audin, L., Jomard, H., Alvarado, A., 2019. Interactions between volcanism and geodynamics in the southern termination of the Ecuadorian arc. Tectonophysics, 751, 54-72.

Bablon, M., Quidelleur, X., Samaniego, P., Le Pennec, J. L., Lahitte, P., Liorzou, C., Hidalgo, S., 2018. Eruptive chronology of Tungurahua volcano (Ecuador) revisited based on new K-Ar ages and geomorphological reconstructions. Journal of Volcanology and Geothermal Research, 357, 378-398.

Bablon, M., Quidelleur, X., Samaniego, P., Le Pennec, J. L., Santamaría, S., Liorzou, C., Eschbach, B., 2020. Volcanic history reconstruction in northern Ecuador: insights for eruptive and erosion rates on the whole Ecuadorian arc. Bulletin of Volcanology, 82(1), 1-23.

Baize, S., Audin, L., Alvarado, A., Jomard, H., Bablon, M., Champenois, J., Le Pennec, J. L., 2020a. Active 961 Tectonics and Earthquake Geology Along the Pallatanga Fault, Central Andes of Ecuador. Frontiers in Earth Science, 8, 193.

Baize, S., Nurminen, F., Sarmiento, A., Dawson, T., Takao, M., Scotti, O., Civico, R., 2020b. A worldwide and Unified Database of Surface Ruptures (SURE) for fault displacement hazard analyses. Seismological Research Letters, 91(1), 499-520.

Barberi, F., Coltelli, M., Ferrara, G., Innocenti, F., Navarro, J. M., Santacroce, R., 1988. Plio-quaternary volcanism in Ecuador. Geological Magazine, 125(1), 1-14.

Beauval, C., Yepes, H., Bakun, W. H., Egred, J., Alvarado, A., Singaucho, J. C., 2010. Locations and magnitudes of historical earthquakes in the Sierra of Ecuador (1587–1996). *Geophysical Journal International*, *181*(3), 1613-1633.

Bellver-Baca, M. T., Chiaradia, M., Beate, B., Beguelin, P., Deriaz, B., Mendez-Chazarra, N., Villagómez, D., 2020. Geochemical evolution of the Quaternary Chachimbiro Volcanic Complex (frontal volcanic arc of Ecuador). *Lithos*, *356*, 105237.

Bernard, B., & Andrade, D. (2011). Volcanes cuaternarios del Ecuador continental. *IGEPN Poster Informativo*.

Bernard, B., Hidalgo, S., Robin, C., Beate, B., Quijozaca, J., 2014. The 3640–3510 BC rhyodacite eruption of Chachimbiro compound volcano, Ecuador: a violent directed blast produced by a satellite dome. Bulletin of Volcanology, 76(9), 1-20.

Boland, M.P., McCourt, W.J., Beate, B., 2000. Mapa geolo´gico de la Cordillera Occidental del Ecuador entre 08–s18N, escala 1/200.000. British Geological Survey-CODIGEM, Direccio´n Nacional de Geologı´a, Quito.

Bourgois, J., 2013. A review on tectonic record of strain buildup and stress release across the Andean forearc along the gulf of Guayaquil-Tumbes basin (GGTB) near Ecuador-Peru border. *International Journal of Geosciences*, *4*, 618-635.

Cassignol, C., Gillot, P.-Y., 1982. Range and effectiveness of unspiked potassium-argon dating: experimental groundwork and application. Odin GS Ed Numer. Dating Stratigr. John Wiley & Sons, New York, 159–179.

Clapperton, C. M., 1990. Glacial and volcanic geomorphology of the Chimborazo-Carihuairazo massif, Ecuadorian Andes. *Earth and Environmental Science Transactions of the Royal Society of Edinburgh*, *81*(2), 91-116.

Cole, J. W., Milner, D. M., Spinks, K. D., 2005. Calderas and caldera structures: a review. Earth-Science Reviews, 69(1-2), 1-26.

Cotten, J., Le Dez, A., Bau, M., Caroff, M., Maury, R. C., Dulski, P., Brousse, R., 1995. Origin of anomalous rare-earth element and yttrium enrichments in subaerially exposed basalts: evidence from French Polynesia. Chemical Geology, 119(1-4), 115-138.

Deino, A., Potts, R., 1992. Age-probability spectra for examination of single-crystal 40Ar39Ar dating results: Examples from Olorgesailie, southern Kenya Rift. Quaternary International, 13, 47-53.

Deligne, N. I., Coles, S. G., Sparks, R. S. J., 2010. Recurrence rates of large explosive volcanic eruptions. Journal of Geophysical Research: Solid Earth, 115(B6).

Deline, P. (2009). Interactions between rock avalanches and glaciers in the Mont Blanc massif during the late Holocene. Quaternary Science Reviews, 28(11-12), 1070-1083.

Dibacto Kamwa, S., 2020. Dynamique de construction et démantèlement des volcans tertiaires et quaternaires des Carpates par des approches géomorphologiques et géochronologiques (Doctoral dissertation, université Paris-Saclay).

Dufresne, A., Siebert, L., Bernard, B., 2021. Distribution and geometric parameters of volcanic debris-avalanche deposits. In Volcanic Debris Avalanches (pp. 75-90). Springer, Cham.

Ego, F., Sébrier, M., Carey-Gailhardis, E., Beate, B., 1996. Do the Billecocha normal faults (Ecuador) reveal extension due to lithospheric body forces in the northern Andes?. *Tectonophysics*, *265*(3-4), 255-273.

Ego, F., Sébrier, M., Lavenu, A., Yepes, H., Egues, A., 1996. Quaternary state of stress in the Northern Andes and the restraining bend model for the Ecuadorian Andes. *Tectonophysics*, *259*(1-3), 101-116.

Eguez, A., Alvarado, A., Yepes, H., Machette, M. N., Costa, C., Dart, R. L., Bradley, L. A., 2003. Database and map of Quaternary faults and folds of Ecuador and its offshore regions. US Geological Survey Open-File Report, 3, 289. doi=10.1.1.593.980

Feininger, T., Bristow, C. R., 1980. Cretaceous and Paleogene geologic history of coastal Ecuador. Geologische Rundschau, 69(3), 849-874.

Germa, A., Lahitte, P., Quidelleur, X., 2015 Construction and destruction of Mont Pelée volcano: volumes and rates constrained from a geomorphological model of evolution: construction and destruction of Mont Pelée. J Geophys Res Earth Surf 120:1206–1226. https://doi.org/10.1002/2014JF003355

Germa, A., Quidelleur, X., Lahitte, P., Labanieh, S., Chauvel, C., 2011. The K–Ar Cassignol– Gillot technique applied to western Martinique lavas: A record of Lesser Antilles arc ACCEPTED MANUSCRIPT ACCEPTED MANUSCRIPT 32 activity from 2 Ma to Mount Pelée volcanism. Quat. Geochronol. 6, 341–355.

Gillot, P.-Y., Hildenbrand, A., Lefèvre, J.-C., Albore-Livadie, C., 2006. The K/Ar dating method: principle, analytical techniques, and application to Holocene volcanic eruptions in Southern Italy. Acta Vulcanol. 18, 55–66.

Goossens, P. J., Rose Jr, W. I., 1973. Chemical composition and age determination of tholeiitic rocks in the basic igneous complex, Ecuador. Geological Society of America Bulletin, 84(3), 1043-1052.

Guillier, B., Chatelain, J. L., Jaillard, E., Yepes, H., Poupinet, G., Fels, J. F., 2001. Seismological evidence on the geometry of the orogenic system in central-northern Ecuador (South America). *Geophysical Research Letters*, *28*(19), 3749-3752.

Gunkel, G., Beulker, C., 2009. Limnology of the Crater Lake Cuicocha, Ecuador, a cold-water tropical lake. International Review of Hydrobiology, 94(1), 103-125.

Gunkel, G., Beulker, C., Grupe, B., Viteri, F., 2009. Survey and assessment of post volcanic activities of a young caldera lake, Lake Cuicocha, Ecuador. Natural Hazards and Earth System Sciences, 9(3), 699.

Gutscher, M.-A., J., Malavieille, S., Lallemand., J.-Y., Collot, 1999, Tectonic segmentation of the North Andean margin: Impact of the Carnegie Ridge collision, Earth Planet. Sci. Lett., 168(3), 255–270.

Hall, M. L., Mothes, P. A., 1994. Tefroestratigrafía holocénica de los volcanes principales del valle interandino, Ecuador. Estudios de geografia, 6, 47-67.

Hall, M. L., & Wood, C. A. (1985). Volcano-tectonic segmentation of the northern Andes. Geology, 13(3), 203-207.

Hall, M. L., Mothes, P. A., Samaniego, P., Militzer, A., Beate, B., Ramón, P., Robin, C., 2017. Antisana volcano: a representative andesitic volcano of the eastern cordillera of Ecuador: petrography, chemistry, tephra, and glacial stratigraphy. *Journal of South American Earth Sciences*, *73*, 50-64.

Hall, M. L., Robin, C., Beate, B., Mothes, P., Monzier, M., 1999. Tungurahua Volcano, Ecuador: structure, eruptive history, and hazards. *Journal of Volcanology and Geothermal Research*, *91*(1), 1-21.

Hall, M. L., Samaniego, P., Le Pennec, J. L., Johnson, J. B., 2008. Ecuadorian Andes volcanism: A review of Late Pliocene to present activity. *Journal of Volcanology and Geothermal Research*, *176*(1), 1-6.

Hall, M., Mothes, P., 2008. The rhyolitic–andesitic eruptive history of Cotopaxi volcano, Ecuador. *Bulletin of Volcanology*, *70*(6), 675-702.

Hall, M., Ramón, P., Mothes, P., Le Pennec, J. L., García, A., Samaniego, P., Yepes, H., 2004. Volcanic eruptions with little warning: the case of Volcán Reventador's Surprise November 3, 2002 Eruption, Ecuador. Revista geológica de Chile, 31(2), 349-358.

Harford, C.L., Pringle, M.S., Sparks, R.S.J., Young, S.R., 2002. The volcanic evolution of Montserrat using 40Ar/39Ar geochronology. Geol. Soc. Lond. Mem. 21, 93–113.

Hidalgo, S., Gerbe, M. C., Martin, H., Samaniego, P., Bourdon, E., 2012. Role of crustal and slab components in the Northern Volcanic Zone of the Andes (Ecuador) constrained by Sr–Nd–O isotopes. Lithos, 132, 180-192.

Hidalgo, S., Monzier, M., Almeida, E., Chazot, G., Eissen, J. P., van der Plicht, J., Hall, M. L., 2008. Late Pleistocene and Holocene activity of the Atacazo–Ninahuilca volcanic complex (Ecuador). *Journal of Volcanology and Geothermal Research*, *176*(1), 16-26.

Hughes, R. A., Pilatasig, L. F., 2002. Cretaceous and Tertiary terrane accretion in the Cordillera Occidental of the Andes of Ecuador. Tectonophysics, 345(1-4), 29-48.

Jaillard, E., Ordonez, M., Suarez, J., Toro, J., Iza, D., Lugo, W., 2004. Stratigraphy of the Late Cretaceous–Paleogene deposits of the cordillera occidental of central Ecuador: geodynamic implications. Journal of South American Earth Sciences, 17(1), 49-58.

Jomard, H., Saqui, D., Baize, S., Alvarado, A., Bernard, B., Audin, L., Hidalgo, S., Pacheco, D., Ruiz, M., Segovia, M., 2021. Interactions between active tectonics and gravitational deformation along with the Billecocha fault system (Northern Ecuador): Insights from morphological and paleoseismological investigations, Journal of South American Earth Sciences. DOI: HTTPS:// doi.org/10.1016/j.jsames.2021.103406.

Kerr, A. C., Aspden, J. A., Tarney, J., Pilatasig, L. F., 2002. The nature and provenance of accreted oceanic terranes in western Ecuador: geochemical and tectonic constraints. Journal of the Geological Society, 159(5), 577-594.

Lahitte, P., Samper, A., Quidelleur, X., 2012. DEM-based reconstruction of southern Basse-Terre volcanoes (Guadeloupe archipelago, FWI): Contribution to the Lesser Antilles Arc construction rates and magma production. Geomorphology, 136(1), 148-164.

Lara, L. E., 2009. The 2008 eruption of the Chaitén Volcano, Chile: a preliminary report. Andean Geology, 36(1), 125-129.

Le Pennec, J. L., Ruiz, A. G., Eissen, J. P., Hall, M. L., Fornari, M., 2011. Identifying potentially active volcanoes in the Andes: Radiometric evidence for late Pleistocene-early Holocene eruptions at Volcán Imbabura, Ecuador. Journal of Volcanology and Geothermal Research, 206(3-4), 121-135.

Legros, F., 2000. Minimum volume of a tephra fallout deposit estimated from a single isopach. Journal of Volcanology and Geothermal Research, 96(1-2), 25-32.

Lipman, P. W. (2000). Calderas. Encyclopedia of volcanoes, 643-662.

Lonsdale, P., 2005. Creation of the Cocos and Nazca plates by fission of the Farallon plate, Tectonophysics, 404(3-4), 237–264, doi:10.1016/j.tecto.2005.05.011.

Luzieux, L. D. A., Heller, F., Spikings, R., Vallejo, C. F., Winkler, W., 2006. Origin and Cretaceous tectonic history of the coastal Ecuadorian forearc between 1 N and 3 S: Paleomagnetic, radiometric and fossil evidence. *Earth and Planetary Science Letters*, *249*(3-4), 400-414.

Madera, L. F., 1918. Ibarra y el terremoto de 1868.

Melián, G. V., Toulkeridis, T., Pérez, N. M., Hernández, P. A., Somoza, L., Padrón, E., Cordero, M., 2021. Geochemistry of Water and Gas Emissions from Cuicocha and Quilotoa Volcanic Lakes, Ecuador. Front. *Earth Sci*, *9*, 741528.

Michaud, F., C. Witt., J. Y. Royer., 2009, Influence of the subduction of the Carnegie volcanic ridge on Ecuadorian geology: Reality and fiction, Geol. Soc. Jpn. Mem., 204, 217–228, doi:10.1130/2009.1204(10).

Monzier, M., Robin, C., Samaniego, P., Hall, M. L., Cotten, J., Mothes, P., Arnaud, N., 1999. Sangay volcano, Ecuador: structural development, present activity, and petrology. *Journal of Volcanology and Geothermal Research*, *90*(1-2), 49-79.

Navarrete, W.F., Le Pennec, J.L., Solano, S., Liorzou, C., Ruiz, G.A., 2020. A first reconstruction of the evolution of Cubilche Volcanic complex, Imbabura Province, Ecuador. J. Volcanol. Geotherm. Res. 406, 107023 https://doi.org/10.1016/j.jvolgeores.2020.107023.

Newhall, C. G., & Punongbayan, R. (Eds.)., 1996. Fire and mud: eruptions and lahars of Mount Pinatubo, Philippines (p. 1126). Quezon City: Philippine Institute of Volcanology and Seismology.

Newhall, C.G., Self, S., 1982. The volcanic explosivity index (VEI) an estimate of explosive magnitude for historical volcanism. J. Geophys. Res.: Oceans 87, 1231–1238.

Nocquet, J. M., Villegas-Lanza, J. C., Chlieh, M., Mothes, P. A., Rolandone, F., Jarrin, P., Yepes, H., 2014. Motion of continental slivers and creeping subduction in the northern Andes. *Nature Geoscience*, *7*(4), 287-291.

Peccerillo, A., Taylor, S.R., 1976. Geochemistry of Eocene calc-alkaline volcanic rocks from the Kastamonu area, northern Turkey. Contrib. Mineral. Petrol. 58, 63–81.

Picuasi, S., Julio, C. 2013. Aportes al Ordenamiento Territorial desde la cosmovisión de los pueblos originarios (Bachelor's thesis).

Pidgen, A., 2014. Cuicocha Volcano, Ecuador: reconstruction of major explosive phases through investigation of associated pyroclastic deposits. Trinity: University of Oxford (Master's thesis).

Pratt, W. T., Duque, P., Ponce, M., 2005. An autochthonous geological model for the eastern Andes of Ecuador. Tectonophysics, 399(1-4), 251-278.

Punongbayan, R. S., Newhall, C. G., Hoblitt, R. P., 1996. Photographic record of rapid geomorphic change at Mount Pinatubo, 1991–94. *Fire and Mud: Eruptions and Lahars of Mount Pinatubo, Philippines*, 21-66.

Reimer, P. J. 2020. Composition and consequences of the IntCal20 radiocarbon calibration curve. Quaternary Research, 96, 22-27.

Reimer, P. J., Bard, E., Bayliss, A., Beck, J. W., Blackwell, P. G., Ramsey, C. B., Van Der Plicht, J., 2013. IntCal13 and Marine13 radiocarbon age calibration curves 0–50,000 years cal BP. *radiocarbon*, *55*(4), 1869-1887.

Ricci, J., Lahitte, P., Quidelleur, X., 2015a. Construction and destruction rates of volcanoes within tropical environment: Examples from the Basse-Terre Island (Guadeloupe, Lesser Antilles). Geomorphology 228, 597–607.

Ricci, J., Quidelleur, X., Lahitte, P., 2015b. Volcanic evolution of central Basse-Terre Island revisited on the basis of new geochronology and geomorphology data. Bull. Volcanol. 77.

Robin, C., Samaniego, P., Le Pennec, J. L., Fornari, M., Mothes, P., Van Der Plicht, J., 2010. New radiometric and petrological constraints on the evolution of the Pichincha volcanic complex (Ecuador). *Bulletin of volcanology*, *72*(9), 1109-1129.

Robin, C., Samaniego, P., Le Pennec, J.L., Fornari, M., Mothes, P., van der Plicht, J., 2010. New radiometric and petrological constraints on the evolution of the Pichincha volcanic complex (Ecuador). Bull. Volcanol. 72, 1109–1129. http://dx.doi.org/10.1007/s00445-010-0389-0

Roverato, M., Dufresne, A., Procter, J., 2021. Volcanic Debris Avalanches.

Roverato, M., Larrea, P., Casado, I., Mulas, M., Béjar, G., Bowman, L., 2018. Characterization of the Cubilche debris avalanche deposit, a controversial case from the northern Andes, Ecuador. *Journal of Volcanology and Geothermal Research*, *360*, 22-35.

Samaniego, P., Barba, D., Robin, C., Fornari, M., Bernard, B., 2012. Eruptive history of Chimborazo volcano (Ecuador): A large, ice-capped and hazardous compound volcano in the Northern Andes. *Journal of Volcanology and Geothermal Research*, *221*, 33-51.

Samaniego, P., Martin, H., Monzier, M., Robin, C., Fornari, M., Eissen, J. P., Cotten, J., 2005. Temporal evolution of magmatism in the Northern Volcanic Zone of the Andes: the geology and petrology of Cayambe Volcanic Complex (Ecuador). Journal of petrology, 46(11), 2225-2252.

Samaniego, P., Monzier, M., Robin, C., Hall, M. L., 1998. Late Holocene eruptive activity at Nevado Cayambe Volcano, Ecuador. *Bulletin of Volcanology*, *59*(7), 451-459.

Samaniego, P., Rivera, M., Mariño, J., Guillou, H., Liorzou, C., Zerathe, S., Scao, V., 2016. The eruptive chronology of the Ampato–Sabancaya volcanic complex (Southern Peru). Journal of Volcanology and Geothermal Research, 323, 110-128.

Samaniego, P., Ordóñez, J., Bablon, M., Hall, M. L., Quidelleur, X., Lahitte, P., Liorzou, C., 2022. The eruptive chronology of the Carihuairazo volcano (Ecuador): Recurrent sector collapses of a Middle Pleistocene stratovolcano of the northern andes. *Journal of South American Earth Sciences*, *116*, 103865.

Samper, A., Quidelleur, X., Lahitte, P., Mollex, D., 2007. Timing of effusive volcanism and collapse events within an oceanic arc island: Basse-Terre, Guadeloupe archipelago (Lesser Antilles Arc). Earth Planet. Sci. Lett. 258, 175–191.

Satake, K., Kate, Y., 2001. The 1741 Oshima-Oshima eruption: extent and volume of submarine debris avalanche. Geophys Res Lett 28(3):427–430

Sierra, D., Hidalgo, S., Almeida, M., Vigide, N., Lamberti, M. C., Proaño, A., Narváez, D. F., 2021. Temporal and spatial variations of CO2 diffuse volcanic degassing on Cuicocha Caldera Lake–Ecuador. *Journal of Volcanology and Geothermal Research*, *411*, 107145.

Singer, B. S., Wijbrans, J. R., Nelson, S. T., Pringle, M. S., Feeley, T. C., Dungan, M. A., 1998. Inherited argon in a Pleistocene andesite lava: $^{40}Ar/^{39}Ar$ incremental-heating and laser-fusion analyses of plagioclase. *Geology*, *26*(5), 427-430.

Spikings, R. A., Winkler, W., Hughes, R. A., Handler, R., 2005. Thermochronology of allochthonous terranes in Ecuador: Unravelling the accretionary and post-accretionary history of the Northern Andes. Tectonophysics, 399(1-4), 195-220.

Stuiver, M., Reimer, P. J., 1993. Extended 14C database and revised CALIB radiocarbon calibration program, Radiocarbon 35, 215-230.

Stuiver, M., Reimer, P.J., Reimer, R.W., 2005. CALIB 5.0. [WWW program and documentation].

Sun, S.-s., McDonough, W.F., 1989. Chemical and isotopic systematics of oceanic basalts: implications for mantle composition and processes. Geol. Soc. Lond. Spec. Publ. 42, 313–345.

Thouret, J.C., Finizola, A., Fornari, M., Suni, J., Legeley-Padovani, A., Frechen, M., 2001. Geology of El Misti volcano nearby the city of Arequipa, Peru. Geol. Soc. Am. Bull. 113, 1593–1610

Trenkamp, R., Kellogg, J. N., Freymueller, J. T., Mora, H. P., 2002. Wide plate margin deformation, southern Central America and northwestern South America, CASA GPS observations. *Journal of South American Earth Sciences*, *15*(2), 157-171.

Troya, R., 1913. Photo from the historical archive of the Central Bank of Ecuador. *Quito, Ecuador. Code*, *95*, F0490.

Troya, R., 1913. Photo from the historical archive of the Central Bank of Ecuador. *Quito, Ecuador. Code*, *95*, F0490.

UN/ISDR ISfDR., 2004. Living with risk: A global review of disaster reduction initiatives, vol 1. United Nations Publications, New York and Geneva, URL http://www.unisdr.org/files/657_lwr1.pdf

Vallejo Vargas, S. X., 2011. *Distribución de las cenizas volcánicas Holocénicas Tardías en la Costa del Ecuador* (Bachelor's thesis, QUITO/EPN/2011).

Vallejo, C., Almagor, S., Romero, C., Herrera, J. L., Escobar, V., Spikings, R. A., Vermeesch, P., 2020. Sedimentology, provenance and radiometric dating of the Silante Formation: Implications for the Cenozoic evolution of the Western Andes of Ecuador. *Minerals*, *10*(10), 929.

Vallejo, C., Spikings, R. A., Horton, B. K., Luzieux, L., Romero, C., Winkler, W., Thomsen, T. B., 2019. Late Cretaceous to Miocene stratigraphy and provenance of the coastal forearc and Western Cordillera of Ecuador: Evidence for accretion of a single oceanic plateau fragment. In *Andean tectonics* (pp. 209-236). Elsevier.

Vallejo, C., Spikings, R. A., Luzieux, L., Winkler, W., Chew, D., Page, L., 2006. The early interaction between the Caribbean Plateau and the NW South American Plate. Terra Nova, 18(4), 264-269.

Vallejo, C., Winkler, W., Spikings, R. A., Luzieux, L., Heller, F., Bussy, F., 2009. Mode and timing ofterrane accretion in theforearc of the Andes in Ecuador. Backbone of the Americas: shallow subduction, plateau uplift, and ridge and terrane collision, 204, 197.

Valverde, V., Mothes, P. A., Beate, B., Bernard, J., 2021. Enormous and far-reaching debris avalanche deposits from Sangay volcano (Ecuador): Multidisciplinary study and modeling the 30-ka sector collapse. *Journal of Volcanology and Geothermal Research*, *411*, 107172.

Van Thournout, F., Hertogen, J., Quevedo, L., 1992. Allochthonous terranes in northwestern Ecuador. *Tectonophysics*, *205*(1-3), 205-221.

Vásconez Müller, A., Cashman, KV., Mitchell, SJ., Vasconez, FJ., 2022. The 2.6–2.3 ka explosive eruptive period of the Pululahua dome complex, Ecuador: insights from pyroclast analysis. Bull Volcanol 84:81. https://doi.org/10.1007/s00445-022-01590-4

Voight, B., Glicken, H., Janda, R. J., Douglass, P. M., 1981. Catastrophic rockslide avalanche of May 18. In: Lipman PW, Mullineaux DR (eds) The 1980 eruptions of Mount St. Helens, Washington, U.S. Geological Survey Professional Papers 1250:347–377

Von Hillebrandt, C., 1989. Estudio geovolcanológico del Complejo Volcánico Cuicocha-Cotacachi y sus aplicaciones. Provincia de Imbabura. Quito: Escuela Politécnica Nacional (Master's thesis).

Von Hillebrandt, C., Hall, M. L., 1988. Mapa de los Peligros Volcánoicos Potenciales Asociados con el Volcán Cuicocha. Esc, 1(50.000).

Whymper, E., 1892. *Travels amongst the Great Andes of the Equator* (Vol. 1). C. Scribner's Sons.

Wilson, M., 1989. Igneous petrogenesis. A global tectonic approach. Chapman and Hall, London, Glasgow, New York, Tokyo, Melbourne, Madras., pp. 51-97. ISBN: 0-412-53310-3

Wolf, T., 1892. Geografía y geología del Ecuador; publicada por órden del supremo gobierno de la república por Teodoro Wolf. Tipografía de FA Brockhaus.

Yepes, H., Audin, L., Alvarado, A., Beauval, C., Aguilar, J., Font, Y., Cotton, F., 2016. A new view for the geodynamics of Ecuador: Implication in seismogenic source definition and seismic hazard assessment. *Tectonics*, *35*(5), 1249-1279.

## SUPPLEMENTARY FIGURES

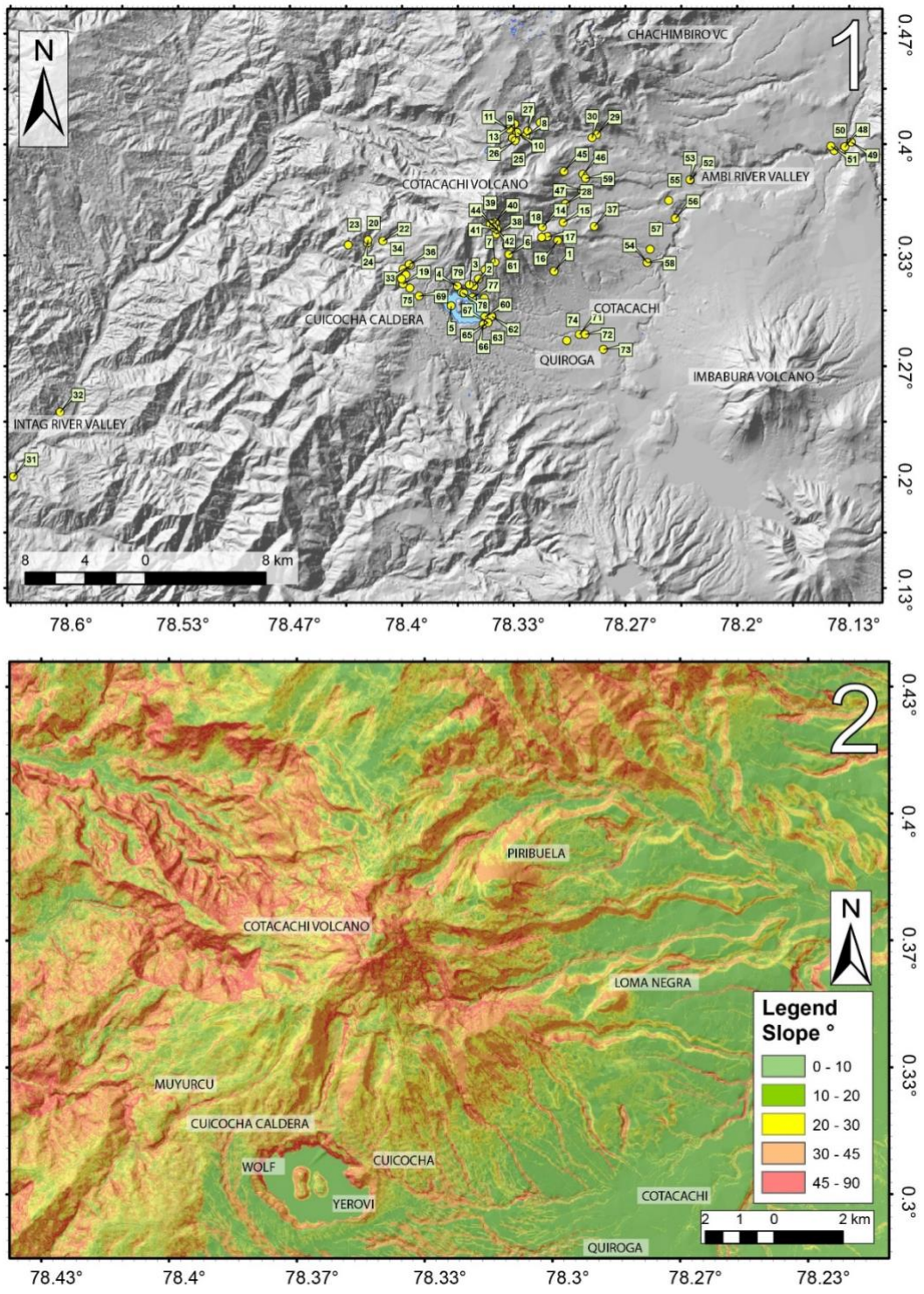


*Figure A 1) Field control points of Cotacachi - Cuicocha volcanic complex, for detailed descriptions of each number, see: Table A. 2) Map of slopes of the area of the Cotacachi - Cuicocha volcanic complex. The map was made using five classes based on the angles of inclination of the slope, expressed in degrees (°).*

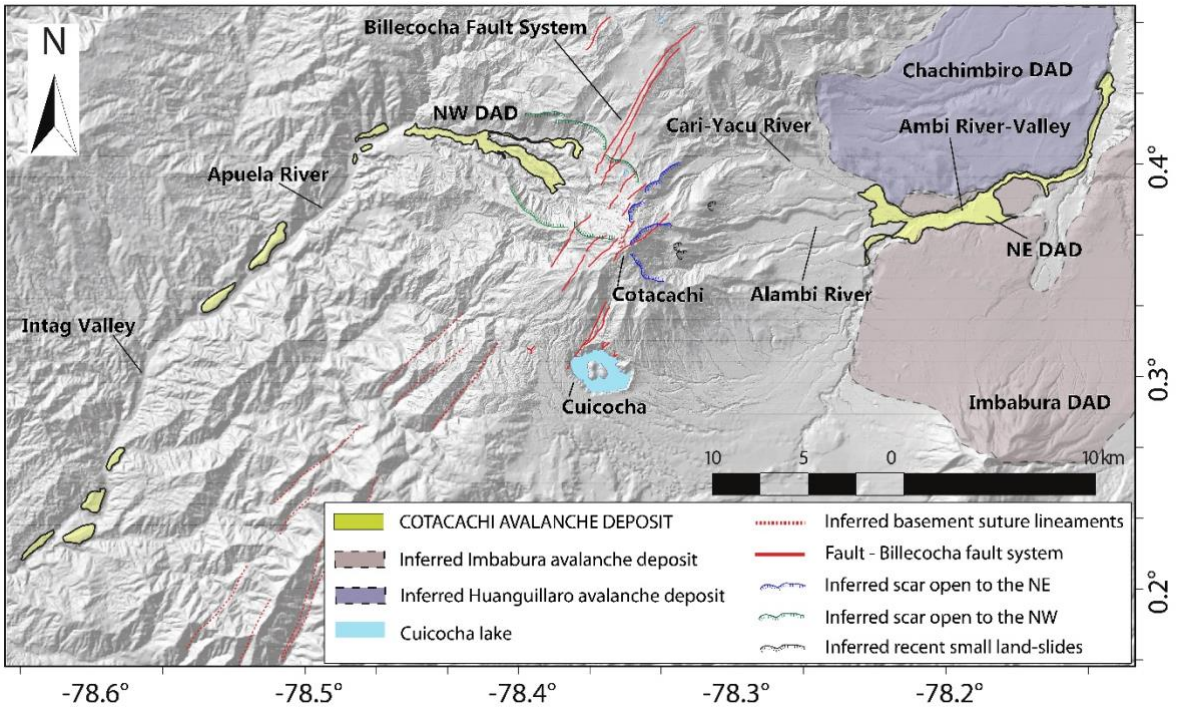


*Figure B. Spatial distribution of the mapped NW and NE avalanche deposits (yellow-colored areas) and possible avalanche scars. Note the Billecocha fault system (Ego, 1996; Eguez et al., 2003; Jomard et al., 2021). crossing the center of the possible avalanche scars. Purple and light brown polygons show the boundaries of the Chachimbiro and Imbabura avalanches. The inferred basement suture lineaments were taken from Boland et al. (2000).*

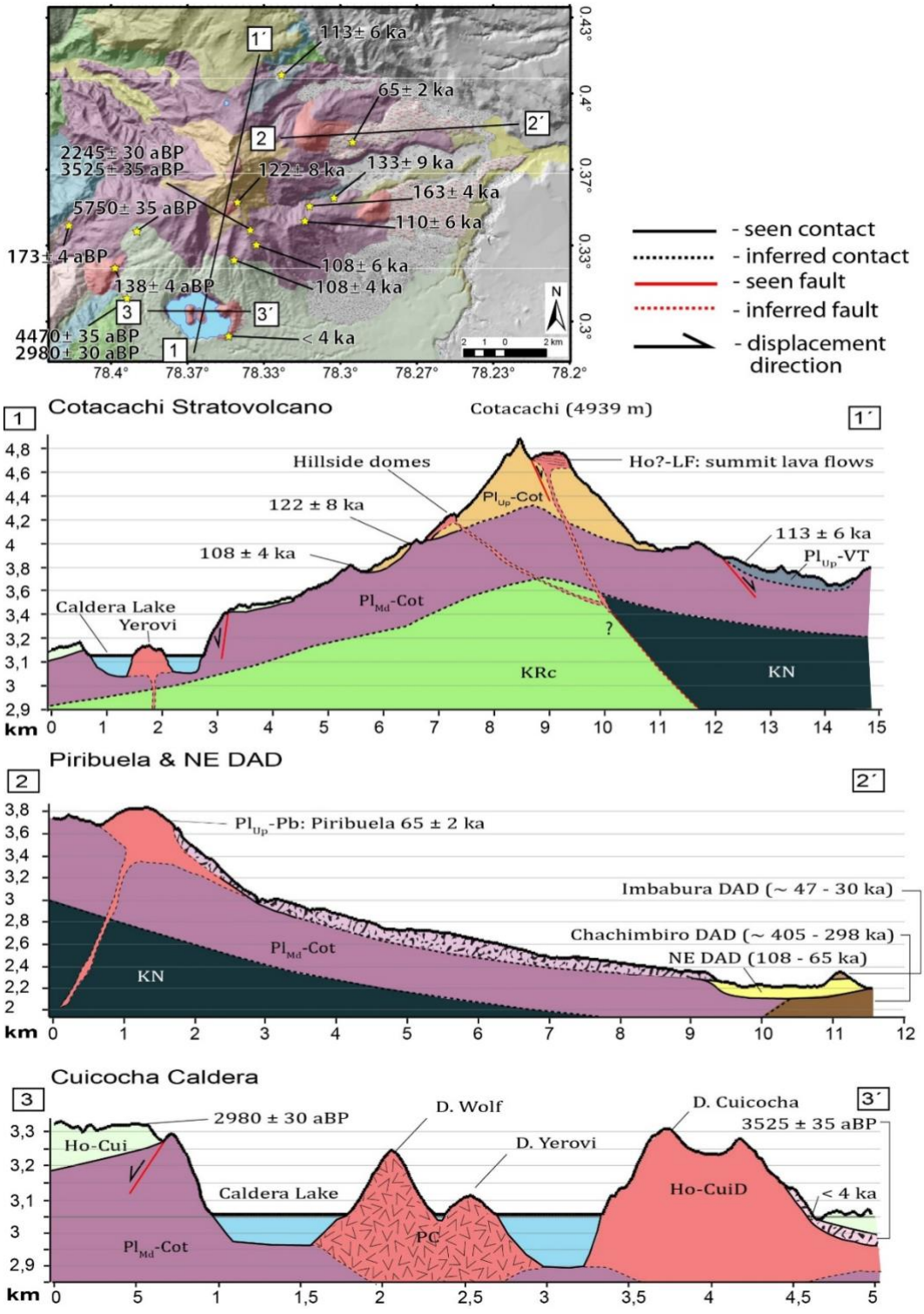


*Figure C. Geological profiles show the spatial distribution of the different stratigraphic members and units. The profiles are adjusted to the observations made during the fieldwork and are consistent with the radiometric and radiocarbon ages obtained during the present study. 1) Profile 1-1´: NNE-SSW longitudinal section along Cotacachi and Cuicocha. 2) Profile 2-2´: Section W-E shows the spatial arrangement of the recent deposits of Piribuela and the avalanche deposits of Cotacachi, Imbabura, and Chachimbiro. 3) Profile 3-3´: Section W-E of the Caldera de Cuicocha.*